SOI: 1.1/TAS DOI: 10.15863/TAS
International Scientific Journal
Theoretical & Applied Science

p-ISSN: 2308-4944 (print) **e-ISSN:** 2409-0085 (online)

Year: 2023 **Issue:** 03 **Volume:** 119

Published: 21.03.2023 **http://T-Science.org**

Issue **Article**

Denis Chemezov
Vladimir Industrial College
M.Sc.Eng., Academician of International Academy of
Theoretical and Applied Sciences, Lecturer, Russian Federation
https://orcid.org/0000-0002-2747-552X
vic-science@yandex.ru

Elizaveta Vorontsova
Vladimir Industrial College
Student, Russian Federation

Dmitriy Netsvetaev
Vladimir Industrial College
Student, Russian Federation

Andrey Volvyankin
Vladimir Industrial College
Student, Russian Federation

Viktor Morozov
Vladimir Industrial College
Student, Russian Federation

Ilya Yakovlev
Vladimir Industrial College
Student, Russian Federation

Denis Korkunov
Vladimir Industrial College
Student, Russian Federation

REFERENCE DATA OF PRESSURE DISTRIBUTION ON THE SURFACES OF AIRFOILS HAVING THE NAMES BEGINNING WITH THE LETTER R

Abstract*: The results of the computer calculation of air flow around the airfoils having the names beginning with the letter R are presented in the article. The contours of pressure distribution on the surfaces of the airfoils at angles of attack of 0, 15 and -15 degrees in conditions of the subsonic airplane flight speed were obtained.*

Key words*: airfoil, angle of attack, pressure, surface.*
Language*: English*
Citation: Chemezov, D., et al. (2023). Reference data of pressure distribution on the surfaces of airfoils having the names beginning with the letter R. *ISJ Theoretical & Applied Science, 03 (119)*, 104-165.
Soi: http://s-o-i.org/1.1/TAS-03-119-20 ***Doi***: crossref https://dx.doi.org/10.15863/TAS.2023.03.119.20
Scopus ASCC*: 1507.*

Introduction

Creating reference materials that determine the most accurate pressure distribution on the airfoil surfaces is an actual task of the airplane aerodynamics.

Materials and methods

The study of air flow around the airfoils was carried out in a two-dimensional formulation by means of the computer calculation in the *Comsol Multiphysics* program. The airfoils in the cross section were taken as objects of research [1-33]. In this work, the airfoils having the names beginning with the letter *R* were adopted. Air flow around the airfoils was carried out at angles of attack (α) of 0, 15 and -15 degrees. Flight speed of the airplane in each case was subsonic. The airplane flight in the atmosphere was carried out under normal weather conditions. The geometric characteristics of the studied airfoils are presented in the Table 1. The geometric shapes of the airfoils in the cross section are presented in the Table 2.

Table 1. The geometric characteristics of the airfoils.

Airfoil name	Max. thickness	Max. camber	Leading edge radius	Trailing edge thickness
R140 12,04% (smoothed)	12.04% at 39.3% of the chord	0.44% at 39.3% of the chord	0.6751%	0.0%
R140 (original)	12.0% at 39.3% of the chord	0.46% at 42.1% of the chord	0.6176%	0.0%
R-3	15.5% at 25.0% of the chord	4.43% at 20.0% of the chord	2.2273%	0.0%
RAE 2822	12.11% at 37.9% of the chord	1.26% at 75.7% of the chord	0.8496%	0.0%
RAE 5214	9.67% at 35.5% of the chord	1.44% at 69.1% of the chord	1.9495%	0.0%
RAE 5215	9.65% at 35.5% of the chord	1.63% at 69.1% of the chord	1.9495%	0.38%
RAE(NPL) 5212	11.95% at 35.5% of the chord	1.83% at 69.1% of the chord	1.3429%	0.0%
RAE(NPL) 5213	9.95% at 35.5% of the chord	1.44% at 69.1% of the chord	1.9495%	0.0%
RAE6-9CK	12.11% at 37.9% of the chord	1.26% at 75.7% of the chord	0.8496%	0.0%
RAF 15	6.49% at 15.0% of the chord	2.61% at 30.0% of the chord	0.8188%	0.0%
RAF 19	10.5% at 15.0% of the chord	10.14% at 40.0% of the chord	1.2276%	0.0%
RAF 25	6.48% at 30.1% of the chord	1.04% at 50.1% of the chord	0.7155%	0.0%
RAF 26	6.62% at 30.0% of the chord	2.14% at 50.0% of the chord	0.6559%	0.0%
RAF 27	9.76% at 30.0% of the chord	0.0% at 0.0% of the chord	0.8931%	0.0%
RAF 28	9.82% at 30.0% of the chord	1.93% at 40.0% of the chord	0.8805%	0.0%
RAF 30	12.64% at 30.0% of the chord	0.0% at 0.0% of the chord	1.3224%	0.0%
RAF 30 MOD	7.6% at 30.0% of the chord	0.0% at 0.0% of the chord	0.7648%	0.0%
RAF 31	12.74% at 30.0% of the chord	2.07% at 50.0% of the chord	1.2741%	0.0%
RAF 32	12.68% at 30.0% of the chord	5.01% at 50.0% of the chord	1.8051%	0.0%
RAF 32 MOD	10.16% at 30.0% of the chord	3.95% at 50.0% of the chord	0.9261%	0.0%
RAF 33	12.64% at 30.0% of the chord	4.69% at 30.0% of the chord	1.4192%	0.0%
RAF 34	12.64% at 30.0% of the chord	2.0% at 30.0% of the chord	1.3033%	0.0%
RAF 38	12.65% at 30.0% of the chord	2.52% at 40.0% of the chord	1.8256%	0.0%
RAF 6	9.98% at 30.0% of the chord	4.59% at 30.0% of the chord	1.6744%	0.3%
RAF 69	20.64% at 30.0% of the chord	1.71% at 50.0% of the chord	3.3379%	0.0%
RAF 89	25.0% at 30.0% of the chord	1.64% at 50.0% of the chord	5.1501%	0.0%
RAF-48	14.96% at 30.0% of the chord	2.93% at 40.0% of the chord	1.7532%	0.0%
REFLEXS1	8.8% at 15.0% of the chord	5.75% at 30.0% of the chord	1.2343%	0.3%
REPUBLIC S-3	11.0% at 30.0% of the chord	1.83% at 15.0% of the chord	0.9011%	0.0%
RG 12A-1,8-9,0	8.99% at 34.4% of the chord	1.8% at 34.4% of the chord	0.5536%	0.0%
RG 14	8.47% at 31.0% of the chord	1.58% at 36.0% of the chord	0.4321%	0.0%
RG 14 10%	10.0% at 31.0% of the chord	1.58% at 36.0% of the chord	1.0017%	0.0%
RG 14 9%	9.0% at 31.0% of the chord	1.58% at 36.0% of the chord	0.864%	0.0%
RG 14 9,5%	9.5% at 31.0% of the chord	1.58% at 36.0% of the chord	0.9301%	0.0%
RG 14A-1,4-7,0	7.0% at 29.8% of the chord	1.4% at 34.4% of the chord	0.4058%	0.0%
RG 15A 2,5-13,0	12.99% at 30.4% of the chord	2.5% at 39.7% of the chord	1.2121%	0.0%
RG 15A-1,8-11,0	11.0% at 30.4% of the chord	1.8% at 39.7% of the chord	0.8897%	0.0%
RG 8	10.78% at 33.6% of the chord	2.22% at 59.4% of the chord	0.7905%	0.0%
RG-12	9.26% at 30.9% of the chord	1.38% at 35.8% of the chord	0.4786%	0.0%
RG-12A	8.99% at 34.4% of the chord	1.8% at 34.4% of the chord	0.5536%	0.0%
RG-14	8.47% at 31.0% of the chord	1.58% at 36.0% of the chord	0.8008%	0.0%
RG14A147	7.0% at 29.8% of the chord	1.4% at 34.4% of the chord	0.4058%	0.0%
RG-15	8.92% at 30.2% of the chord	1.76% at 40.3% of the chord	0.6885%	0.0%
RG-15 8,9%	8.92% at 30.2% of the chord	1.76% at 40.3% of the chord	0.4852%	0.0%
RG-8	10.78% at 33.6% of the chord	2.22% at 59.4% of the chord	0.7102%	0.0%
Rhode St Genese 26	10.0% at 30.0% of the chord	5.0% at 30.0% of the chord	0.5652%	0.0%
Rhode St Genese 28	7.58% at 30.0% of the chord	3.79% at 30.0% of the chord	0.8187%	0.0%
Rhode St Genese 29	8.66% at 30.0% of the chord	4.33% at 30.0% of the chord	0.9046%	0.0%
Rhode St Genese 30	9.74% at 30.0% of the chord	4.87% at 30.0% of the chord	0.9234%	0.0%
Rhode St Genese 31	10.82% at 30.0% of the chord	5.41% at 30.0% of the chord	1.2494%	0.0%

Rhode St Genese 32	11.9% at 30.0% of the chord	5.95% at 30.0% of the chord	1.5398%	0.0%
Ritz 1-30-10	10.0% at 30.0% of the chord	1.0% at 30.0% of the chord	0.9454%	0.2%
Ritz 1-30-11	11.0% at 30.0% of the chord	1.0% at 30.0% of the chord	1.0825%	0.22%
Ritz 1-30-12	12.0% at 30.0% of the chord	1.0% at 30.0% of the chord	1.2419%	0.24%
Ritz 1-30-13	13.0% at 30.0% of the chord	1.0% at 30.0% of the chord	1.4229%	0.26%
Ritz 1-30-14	14.0% at 30.0% of the chord	1.0% at 30.0% of the chord	1.6245%	0.28%
Ritz 1-30-15	15.0% at 30.0% of the chord	1.0% at 30.0% of the chord	1.8462%	0.3%
Ritz 1-30-5	5.0% at 30.0% of the chord	1.0% at 30.0% of the chord	0.6166%	0.1%
Ritz 1-30-6	6.0% at 30.0% of the chord	1.0% at 30.0% of the chord	0.6355%	0.12%
Ritz 1-30-7	7.0% at 30.0% of the chord	1.0% at 30.0% of the chord	0.6767%	0.14%
Ritz 1-30-8	8.0% at 30.0% of the chord	1.0% at 30.0% of the chord	0.7419%	0.16%
Ritz 1-30-9	9.0% at 30.0% of the chord	1.0% at 30.0% of the chord	0.8316%	0.18%
Ritz 2-30-10	10.0% at 30.0% of the chord	2.0% at 30.0% of the chord	0.9454%	0.2%
Ritz 2-30-11	11.0% at 30.0% of the chord	2.0% at 30.0% of the chord	1.0825%	0.22%
Ritz 2-30-12	12.0% at 30.0% of the chord	2.0% at 30.0% of the chord	1.0111%	0.2%
Ritz 2-30-13	13.0% at 30.0% of the chord	2.0% at 30.0% of the chord	1.4229%	0.26%
Ritz 2-30-14	14.0% at 30.0% of the chord	2.0% at 30.0% of the chord	1.6245%	0.28%
Ritz 2-30-15	15.0% at 30.0% of the chord	2.0% at 30.0% of the chord	1.8462%	0.3%
Ritz 2-30-5	5.0% at 30.0% of the chord	2.0% at 30.0% of the chord	0.6166%	0.1%
Ritz 2-30-6	6.0% at 30.0% of the chord	2.0% at 30.0% of the chord	0.6355%	0.12%
Ritz 2-30-7	7.0% at 30.0% of the chord	2.0% at 30.0% of the chord	0.6767%	0.14%
Ritz 2-30-8	8.0% at 30.0% of the chord	2.0% at 30.0% of the chord	0.7419%	0.16%
Ritz 2-30-9	9.0% at 30.0% of the chord	2.0% at 30.0% of the chord	0.8316%	0.18%
Ritz 3-30-10	10.0% at 30.0% of the chord	3.0% at 30.0% of the chord	0.8648%	0.2%
Ritz 3-30-11	11.0% at 30.0% of the chord	3.0% at 30.0% of the chord	0.9873%	0.22%
Ritz 3-30-12	12.0% at 30.0% of the chord	3.0% at 30.0% of the chord	1.1291%	0.24%
Ritz 3-30-13	13.0% at 30.0% of the chord	3.0% at 30.0% of the chord	1.2897%	0.26%
Ritz 3-30-14	14.0% at 30.0% of the chord	3.0% at 30.0% of the chord	1.4686%	0.28%
Ritz 3-30-15	15.0% at 30.0% of the chord	3.0% at 30.0% of the chord	1.6654%	0.3%
Ritz 3-30-5	5.0% at 30.0% of the chord	3.0% at 30.0% of the chord	0.5337%	0.1%
Ritz 3-30-6	6.0% at 30.0% of the chord	3.0% at 30.0% of the chord	0.5638%	0.12%
Ritz 3-30-7	7.0% at 30.0% of the chord	3.0% at 30.0% of the chord	0.6118%	0.14%
Ritz 3-30-8	8.0% at 30.0% of the chord	3.0% at 30.0% of the chord	0.6775%	0.16%
Ritz 3-30-9	9.0% at 30.0% of the chord	3.0% at 30.0% of the chord	0.7616%	0.18%
RK40	8.48% at 36.6% of the chord	2.12% at 41.9% of the chord	0.3973%	0.0%
Roma 701	10.96% at 30.0% of the chord	5.92% at 30.0% of the chord	2.1712%	0.0%
RONCZ LOW DRAG FLYING WING	12.05% at 42.2% of the chord	2.8% at 38.4% of the chord	0.7781%	0.4034%
Roncz/Marske-7	12.05% at 42.2% of the chord	2.8% at 38.4% of the chord	0.7795%	0.404%
rs001	9.83% at 25.0% of the chord	1.64% at 34.5% of the chord	0.7693%	0.0%
rs001m05	9.92% at 25.9% of the chord	0.82% at 34.5% of the chord	0.7167%	0.0%
Rs001m60	9.93% at 25.9% of the chord	0.66% at 34.5% of the chord	0.7197%	0.0%
Rs001m75	9.96% at 25.9% of the chord	0.41% at 34.5% of the chord	0.7236%	0.0%
rs001t10	9.99% at 25.0% of the chord	0.03% at 44.8% of the chord	0.8032%	0.0%
rs004a	8.99% at 25.0% of the chord	1.64% at 34.5% of the chord	0.6676%	0.0%
RSG-28	7.58% at 30.0% of the chord	3.79% at 30.0% of the chord	0.8187%	0.0%
RSG-29	8.66% at 30.0% of the chord	4.33% at 30.0% of the chord	0.9046%	0.0%
RSG-30	9.74% at 30.0% of the chord	4.87% at 30.0% of the chord	0.9234%	0.0%
RSG-31	10.82% at 30.0% of the chord	5.41% at 30.0% of the chord	1.2494%	0.0%
RSG-32	11.9% at 30.0% of the chord	5.95% at 30.0% of the chord	1.5398%	0.0%
RSG-34	14.07% at 30.0% of the chord	7.03% at 30.0% of the chord	2.2251%	0.0%
RSG-36	16.23% at 30.0% of the chord	8.12% at 30.0% of the chord	2.8549%	0.0%
RSG-82	7.58% at 30.0% of the chord	3.79% at 30.0% of the chord	0.8102%	0.0%
Rutan AMSOIL racer canard airfoil	11.62% at 39.0% of the chord	2.08% at 42.0% of the chord	2.1697%	0.442%
Rutan AMSOIL racer wing airfoil	11.76% at 39.0% of the chord	0.97% at 48.0% of the chord	2.143%	0.448%
RUTAN CANARD	11.62% at 39.0% of the chord	2.08% at 42.0% of the chord	2.1697%	0.442%
RUTAN WING	11.76% at 39.0% of the chord	0.97% at 48.0% of the chord	2.143%	0.448%
Ryan BQM-34	9.9% at 32.5% of the chord	0.0% at 0.0% of the chord	1.0353%	0.0%
RYAN BQM-34 FIREBEE WING	9.9% at 32.5% of the chord	0.0% at 0.0% of the chord	1.0335%	0.0%

Note:
RAE (The Royal Aeronautical Establishment in Britain);
RAF (The National Physical Laboratories in Britain);
R140 (original) (R140 Quickee 500 airfoil);
REPUBLIC S-3 (P-47 wing airfoil);
RG 14 (Rolf Girsberger RG 14 airfoil);

Rhode St Genese 26, Rhode St Genese 28, Rhode St Genese 29, Rhode St Genese 30, Rhode St Genese 31, Rhode St Genese 32 (Rhode St. Genese (Belgium));
Ritz 1-30-10, Ritz 1-30-11, Ritz 1-30-12, Ritz 1-30-13, Ritz 1-30-14, Ritz 1-30-15, Ritz 1-30-5, Ritz 1-30-6, Ritz 1-30-7, Ritz 1-30-8, Ritz 1-30-9, Ritz 2-30-10, Ritz 2-30-11, Ritz 2-30-12, Ritz 2-30-13, Ritz 2-30-14, Ritz 2-30-15, Ritz 2-30-5, Ritz 2-30-6, Ritz 2-30-7, Ritz 2-30-8, Ritz 2-30-9, Ritz 3-30-10, Ritz 3-30-11, Ritz 3-30-12, Ritz 3-30-13, Ritz 3-30-14, Ritz 3-30-15, Ritz 3-30-5, Ritz 3-30-6, Ritz 3-30-7, Ritz 3-30-8, Ritz 3-30-9 (F. Ritz (Germany));
RK40 (Ralf Kornmann (racer F5D electrique champion du monde 2000));
Roma 701 (DGA (Italy));
Roncz/Marske-7 (Low drag flying wing);
Rs001m60, Rs001m75 ((c)Reinhard Sielemann);
Ryan BQM-34 (Firebee wing airfoil (NACA 63-014A W/NACA 0014 nose and thinned to .09899 to account for sweep)).

Table 2. The geometric shapes of the airfoils in the cross section.

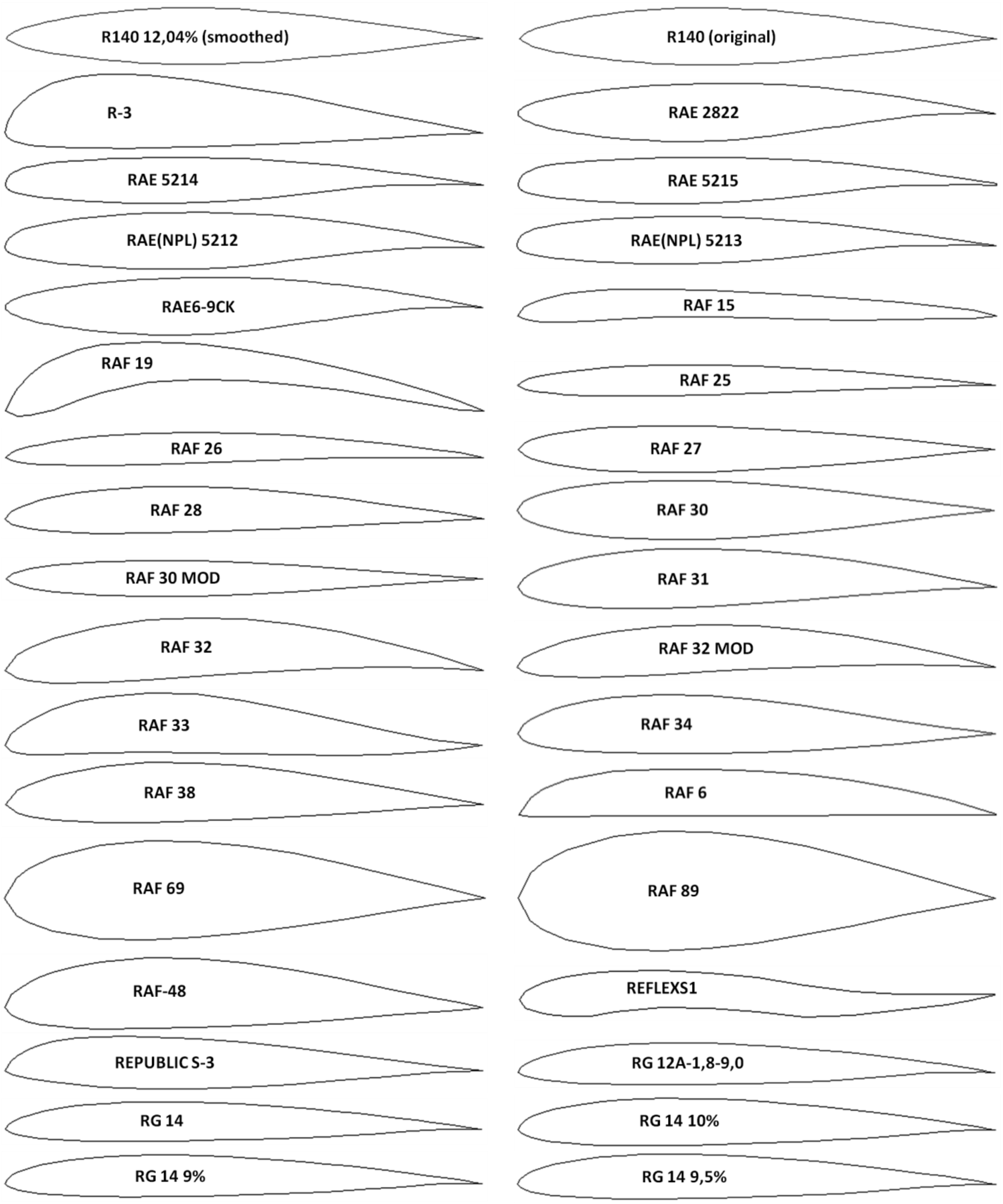

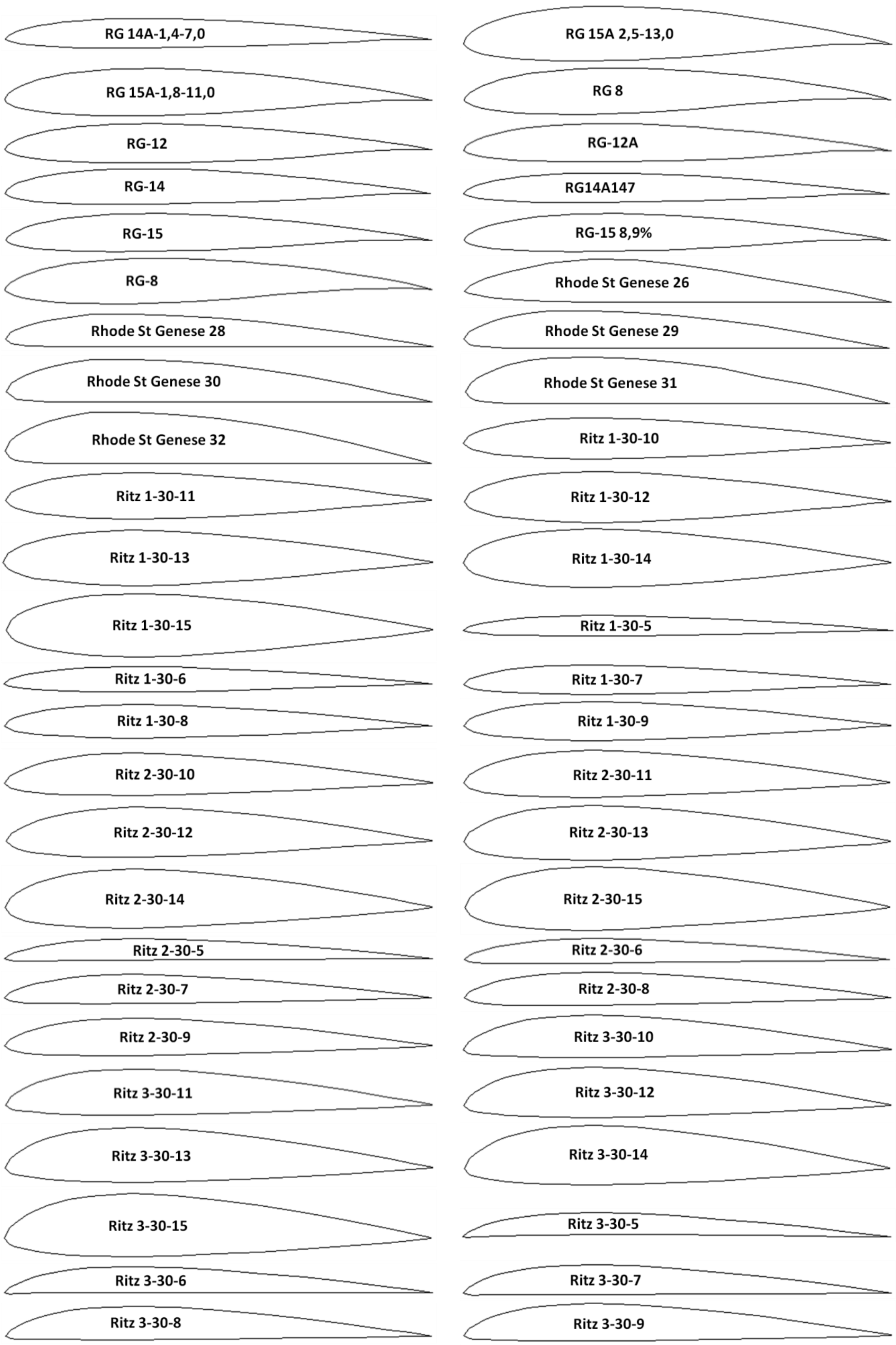

RG 14A-1,4-7,0
RG 15A 2,5-13,0
RG 15A-1,8-11,0
RG 8
RG-12
RG-12A
RG-14
RG14A147
RG-15
RG-15 8,9%
RG-8
Rhode St Genese 26
Rhode St Genese 28
Rhode St Genese 29
Rhode St Genese 30
Rhode St Genese 31
Rhode St Genese 32
Ritz 1-30-10
Ritz 1-30-11
Ritz 1-30-12
Ritz 1-30-13
Ritz 1-30-14
Ritz 1-30-15
Ritz 1-30-5
Ritz 1-30-6
Ritz 1-30-7
Ritz 1-30-8
Ritz 1-30-9
Ritz 2-30-10
Ritz 2-30-11
Ritz 2-30-12
Ritz 2-30-13
Ritz 2-30-14
Ritz 2-30-15
Ritz 2-30-5
Ritz 2-30-6
Ritz 2-30-7
Ritz 2-30-8
Ritz 2-30-9
Ritz 3-30-10
Ritz 3-30-11
Ritz 3-30-12
Ritz 3-30-13
Ritz 3-30-14
Ritz 3-30-15
Ritz 3-30-5
Ritz 3-30-6
Ritz 3-30-7
Ritz 3-30-8
Ritz 3-30-9

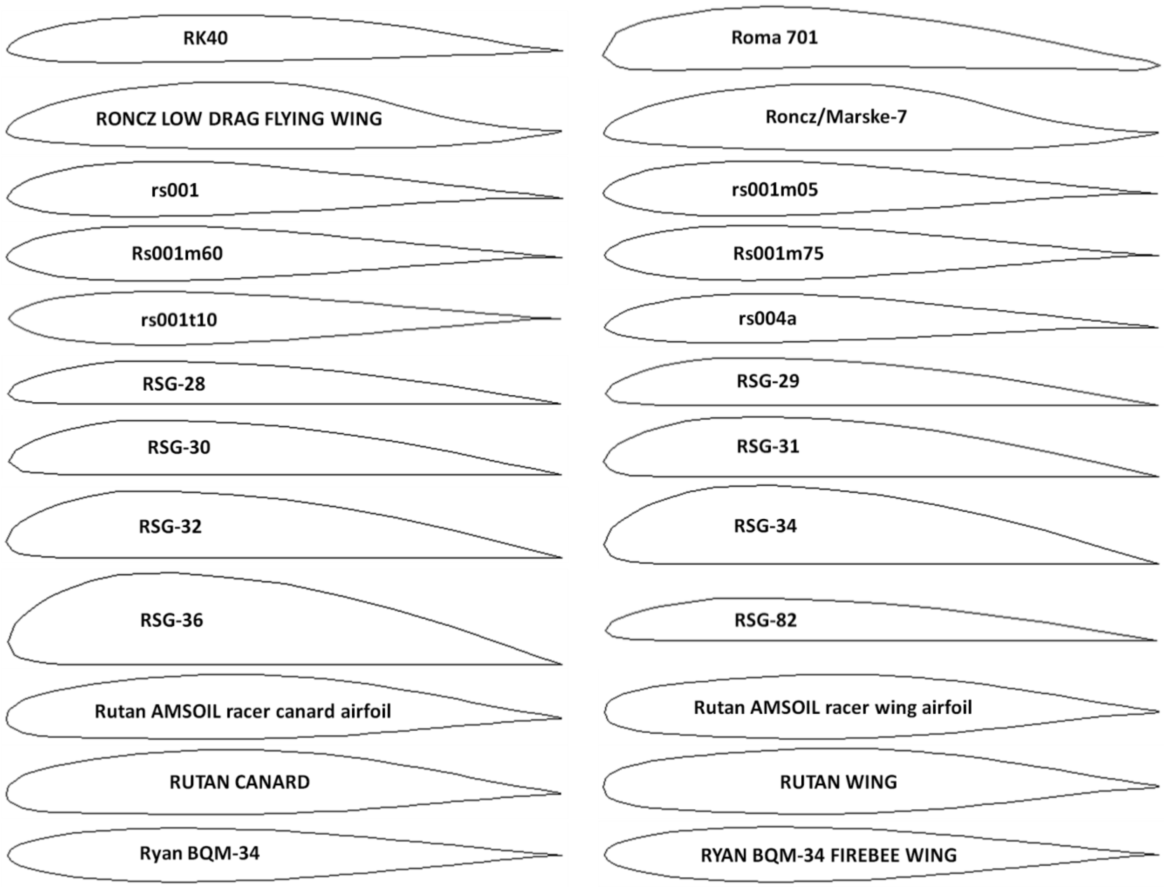

Results and discussion

The calculated pressure contours on the surfaces of the airfoils at different angles of attack are presented in the Figs. 1-108. The calculated values on the scale can be represented as the basic values when comparing the pressure drop under conditions of changing the angle of attack of the airfoils.

108 airfoils of RAE, RAF, RG, Ritz, RSG types and others were considered in this article. All airfoils are asymmetrical, with the exception of the RAF 27, RAF 30, RAF 30 MOD and RYAN BQM-34 (RYAN BQM-34 FIREBEE WING).

The largest and smallest thicknesses of the studied airfoils are 25% and 5% for RAF 89 and Ritz 1-30-5, Ritz 2-30-5 and Ritz 3-30-5, respectively. The largest and smallest cambers are 10.14% and 0.0% for the RAF 19 and all symmetrical airfoils, respectively. The largest and smallest leading edge radii are 5.1501% and 0.4058% for the RAF 89 and RG 14A-1,4-7,0, respectively. The largest and smallest trailing edge thicknesses are 0.448% and 0.0% for the Rutan AMSOIL racer wing and most airfoils, respectively.

Let us consider in detail the aerodynamic characteristics of some airfoils: R-3, RAF 15, RAF 33, REFLEXS1, Rhode St Genese 26, Ritz 2-30-5, Roncz/Marske-7 and RUTAN WING.

In the conditions of the airplane climb, the convex upper surface of the R-3 airfoil reduces the negative pressure on the surface by two times, compared with the airplane descent maneuver. The pressure difference on the upper and lower surfaces of the airfoil can be 1:4. The bulge on the upper surface ensures the formation of a negative pressure gradient in magnitude greater than the positive pressure at zero, positive and negative angles of attack.

Negative pressure on the leading edge increases up to 30 times when the angle of attack of the RAF 15 airfoil increases from 0 to 15 degrees. At the same time, changing the angle of attack to -15 degrees leads to an increase in pressure by 8 times. The horizontal position of the airfoil provides the pressure difference on the surfaces up to 1:2.5.

The location of the maximum thickness of the RAF 33 airfoil in the middle of the chord length is characterized by an increase in negative pressure during the airplane climb. Some camber of the airfoil from the trailing edge affects the formation of air flows at angles of attack of 0 and -15 degrees.

The REFLEXS1 airfoil is characterized by a large drag on the leading edge at an angle of attack of 15 degrees. The configuration of the front part of the airfoil contributes to the formation of pressure gradients of the same intensity on the upper and lower surfaces at angles of attack of 15 and -15 degrees.

The geometric shape of the upper surface of the Rhode St Genese 26 airfoil distributes the maximum negative pressure over the entire surface in the horizontal flight conditions.

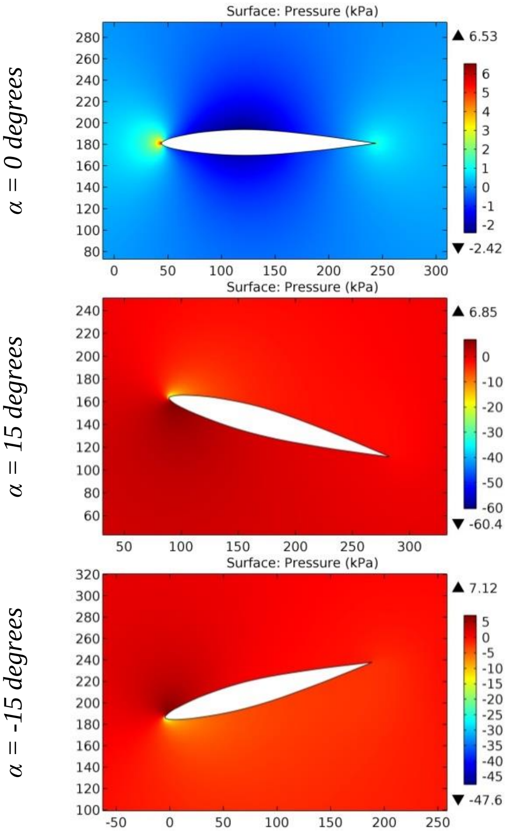

Figure 1. The pressure contours on the surfaces of the R140 12,04% (smoothed) airfoil.

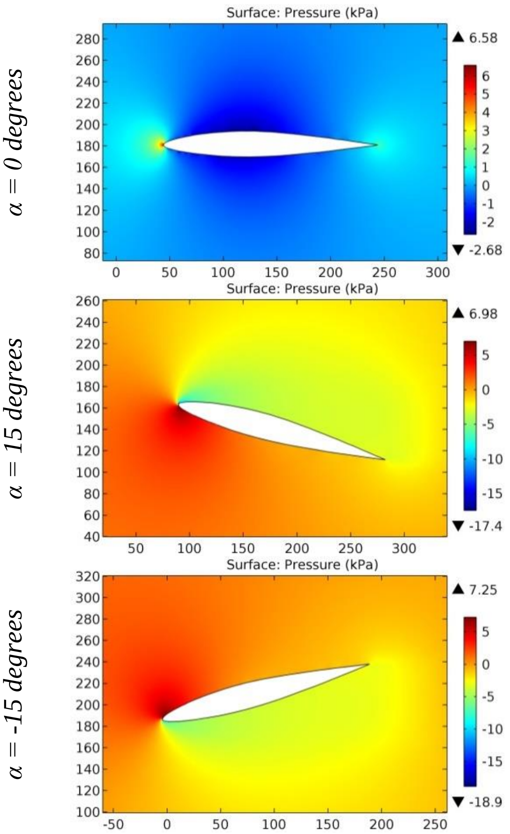

Figure 2. The pressure contours on the surfaces of the R140 (original) airfoil.

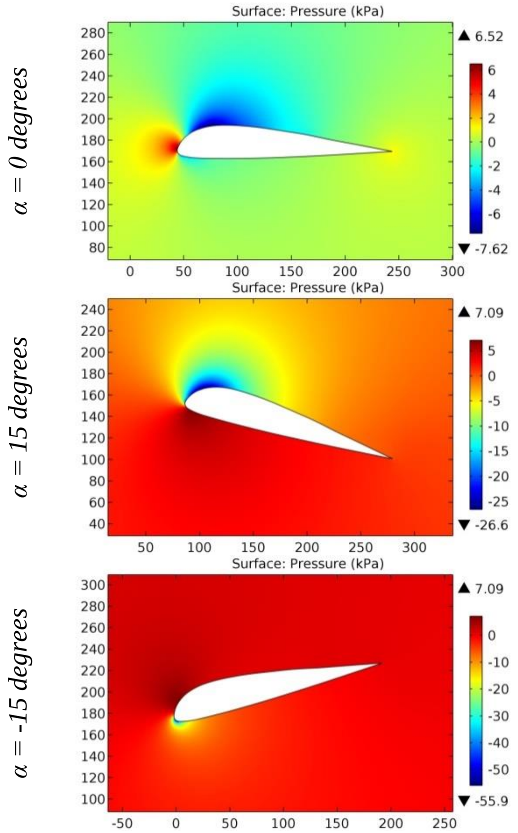

Figure 3. The pressure contours on the surfaces of the R-3 airfoil.

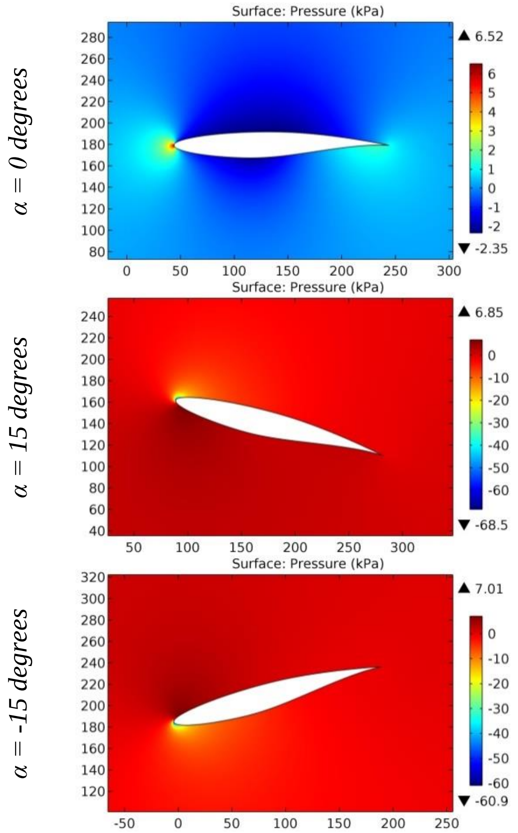

Figure 4. The pressure contours on the surfaces of the RAE 2822 airfoil.

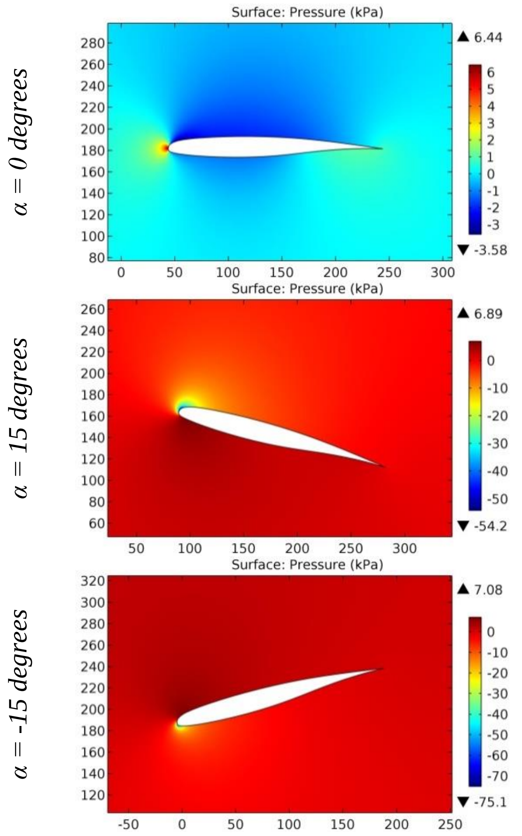

Figure 5. The pressure contours on the surfaces of the RAE 5214 airfoil.

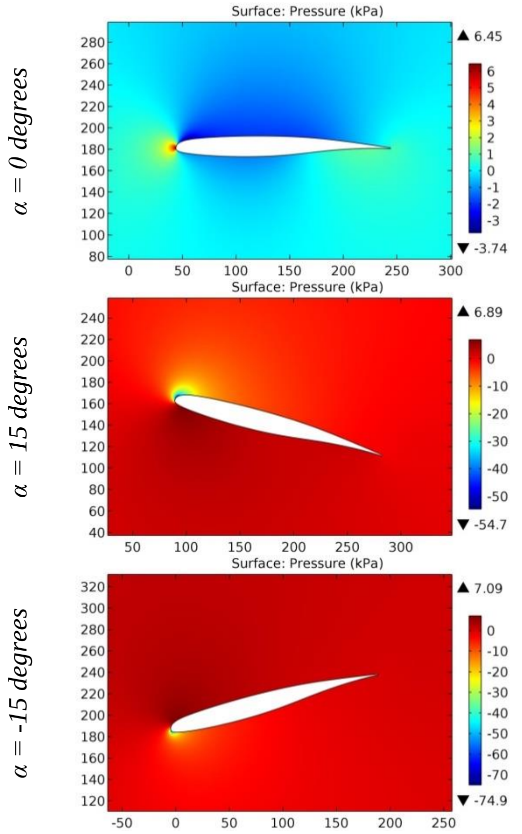

Figure 6. The pressure contours on the surfaces of the RAE 5215 airfoil.

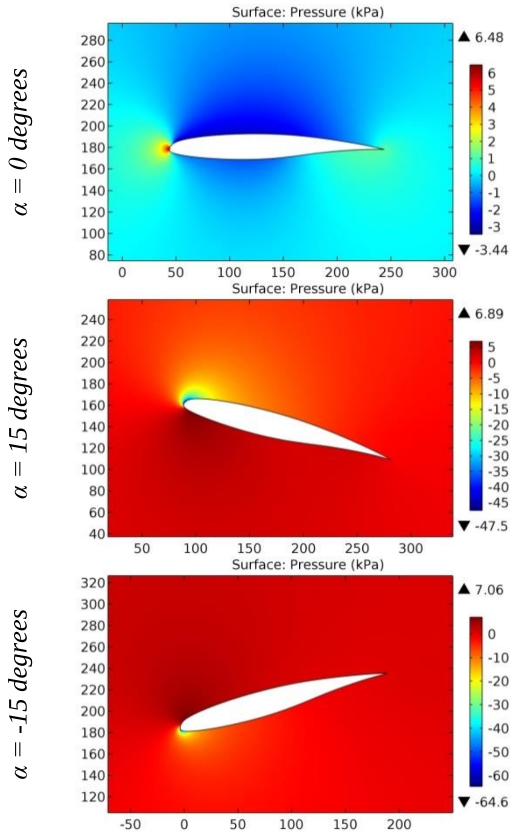

Figure 7. The pressure contours on the surfaces of the RAE(NPL) 5212 airfoil.

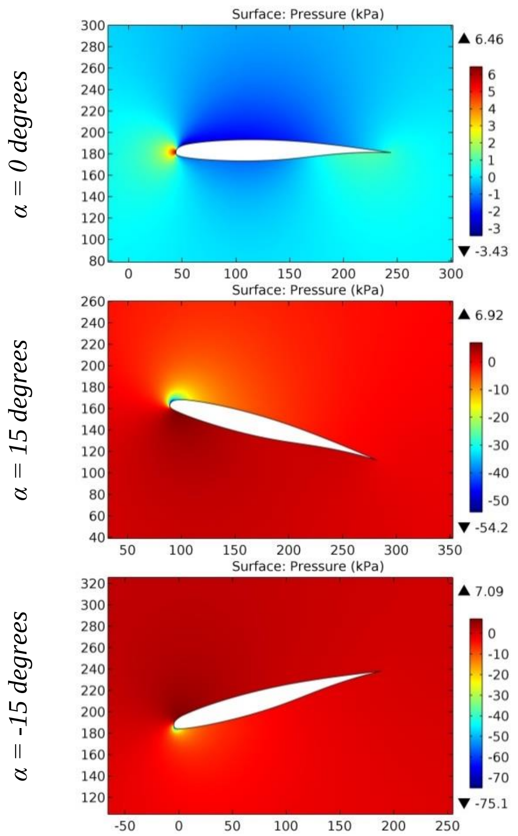

Figure 8. The pressure contours on the surfaces of the RAE(NPL) 5213 airfoil.

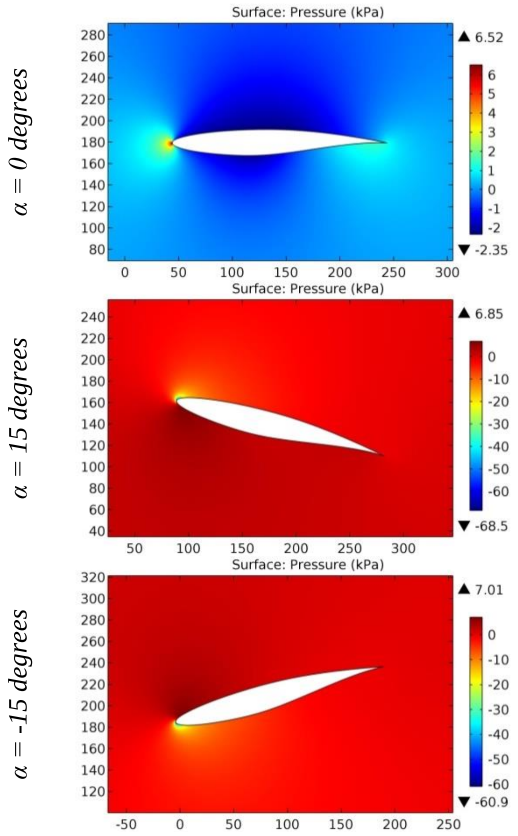

Figure 9. The pressure contours on the surfaces of the RAE6-9CK airfoil.

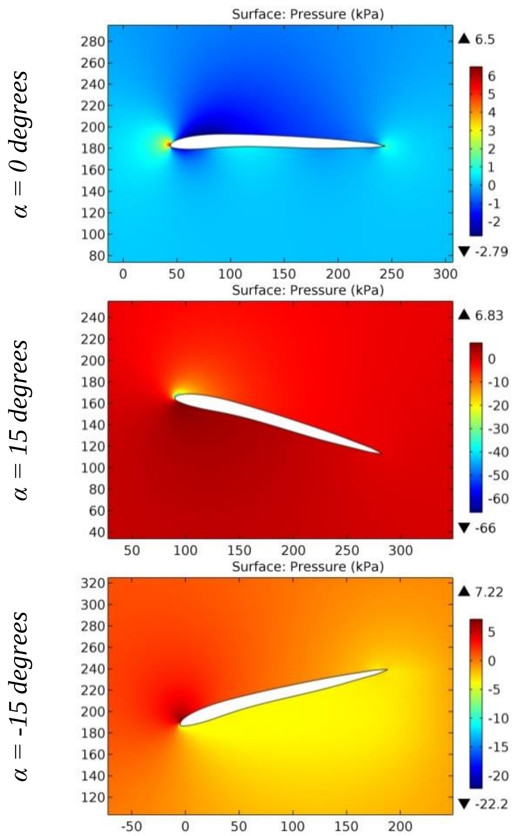

Figure 10. The pressure contours on the surfaces of the RAF 15 airfoil.

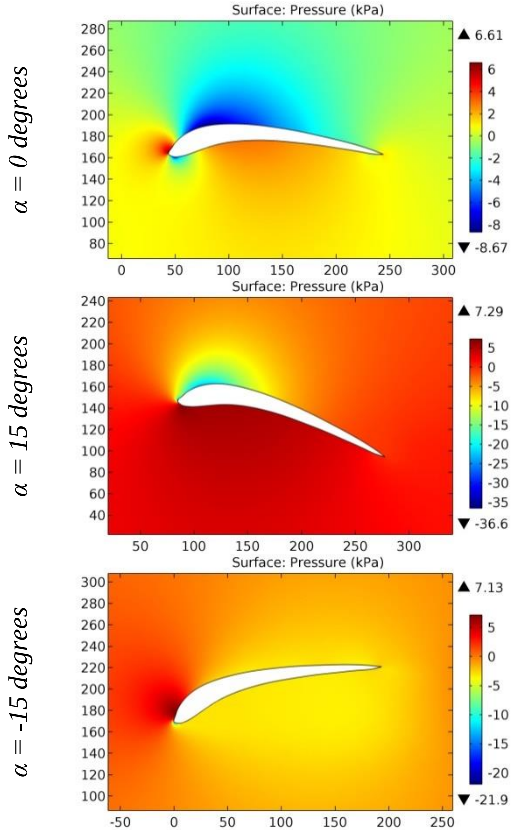

Figure 11. The pressure contours on the surfaces of the RAF 19 airfoil.

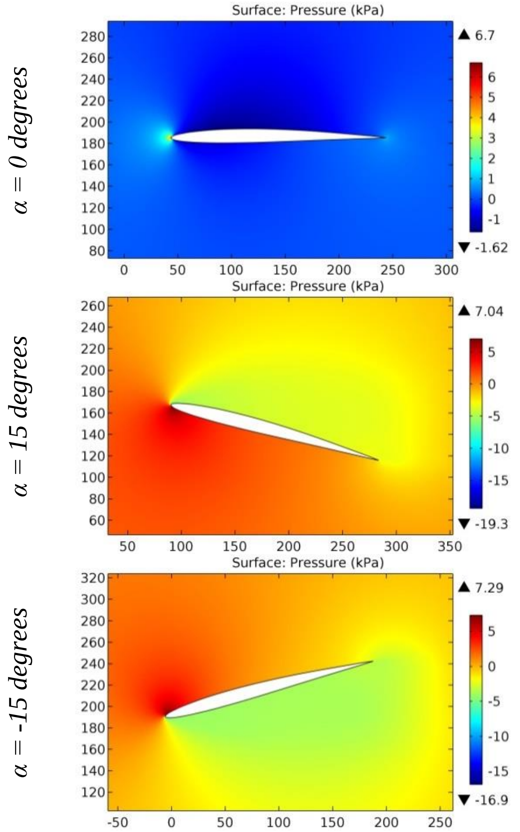

Figure 12. The pressure contours on the surfaces of the RAF 25 airfoil.

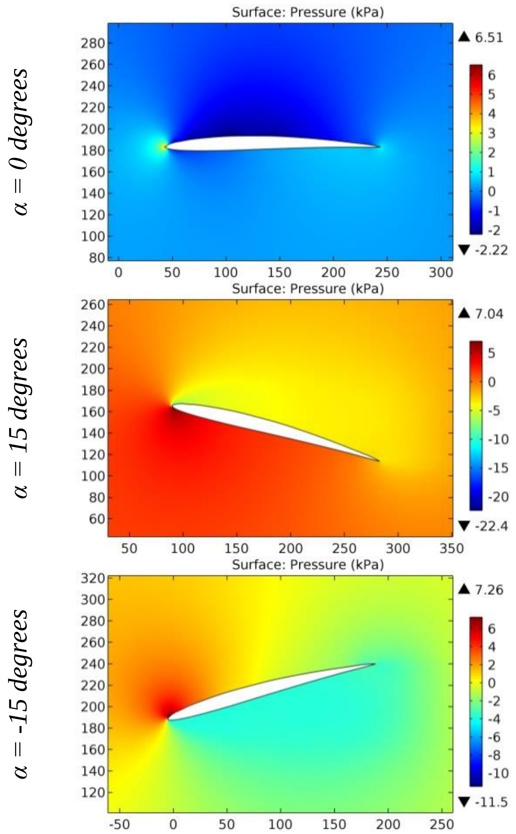

Figure 13. The pressure contours on the surfaces of the RAF 26 airfoil.

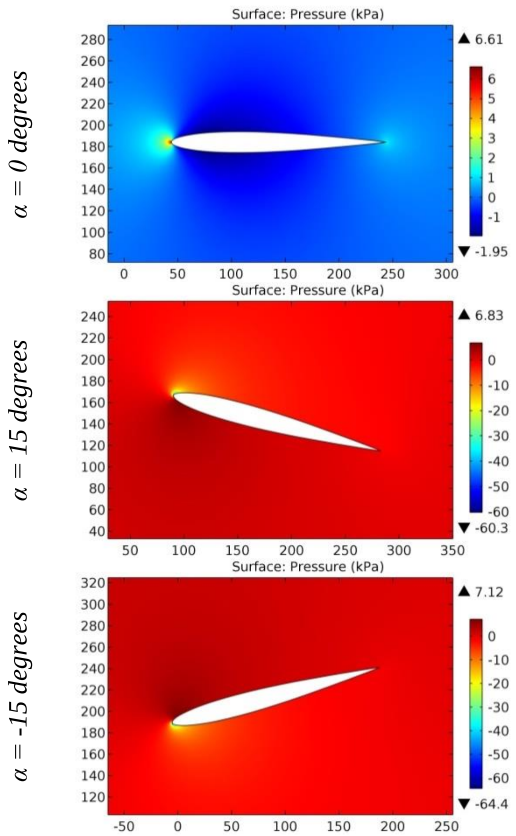

Figure 14. The pressure contours on the surfaces of the RAF 27 airfoil.

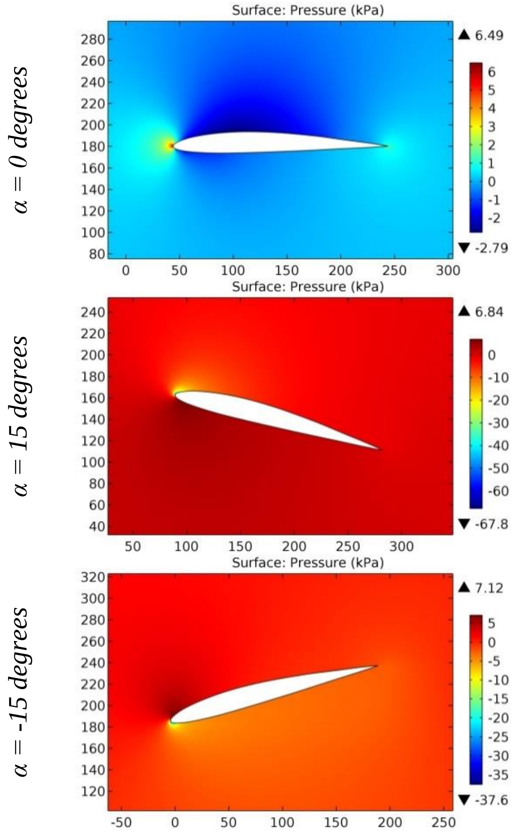

Figure 15. The pressure contours on the surfaces of the RAF 28 airfoil.

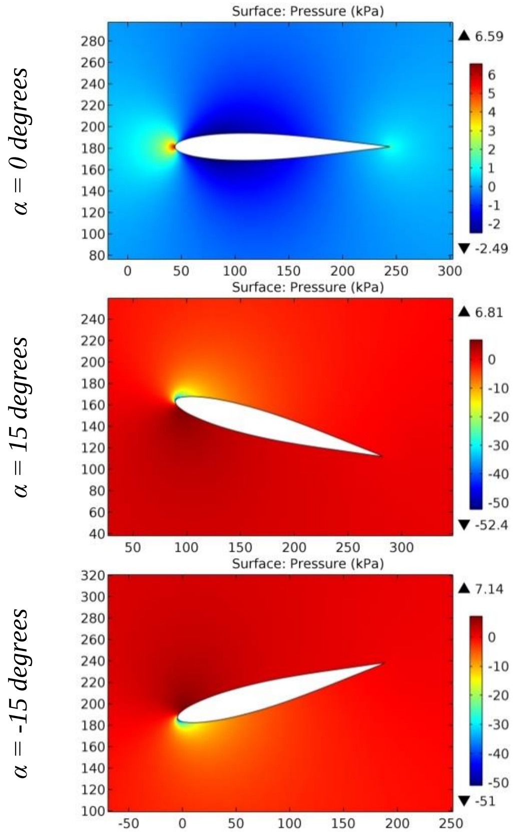

Figure 16. The pressure contours on the surfaces of the RAF 30 airfoil.

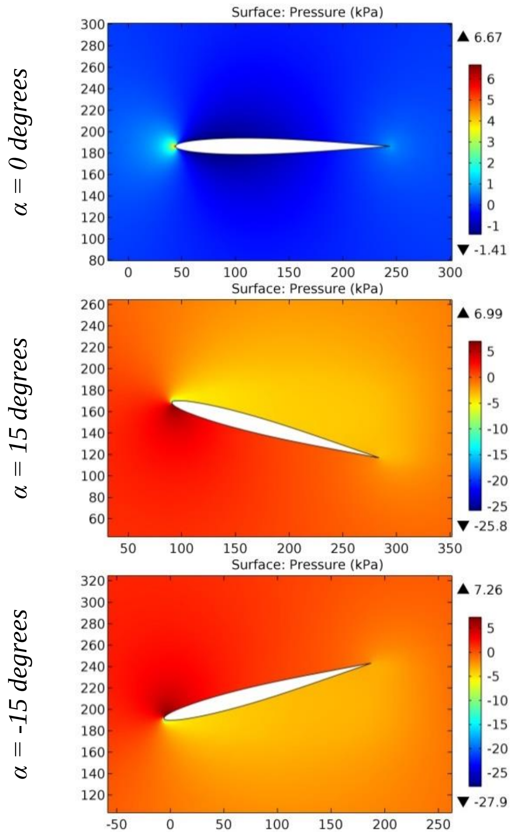

Figure 17. The pressure contours on the surfaces of the RAF 30 MOD airfoil.

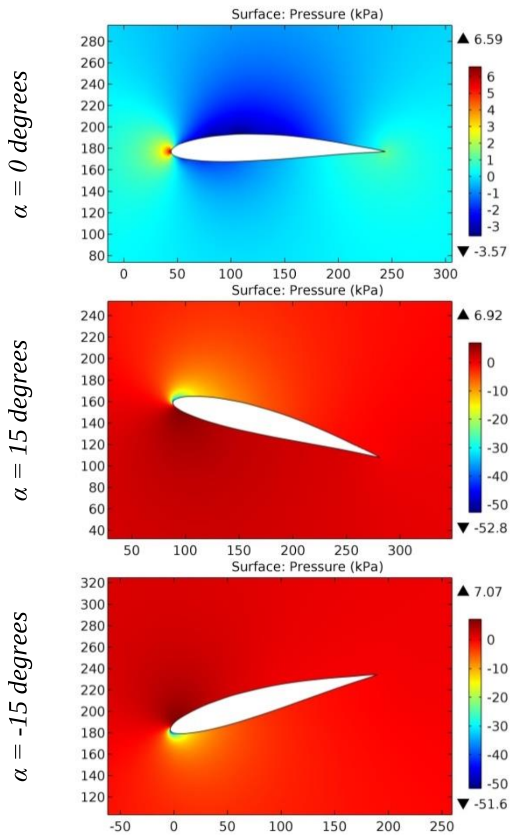

Figure 18. The pressure contours on the surfaces of the RAF 31 airfoil.

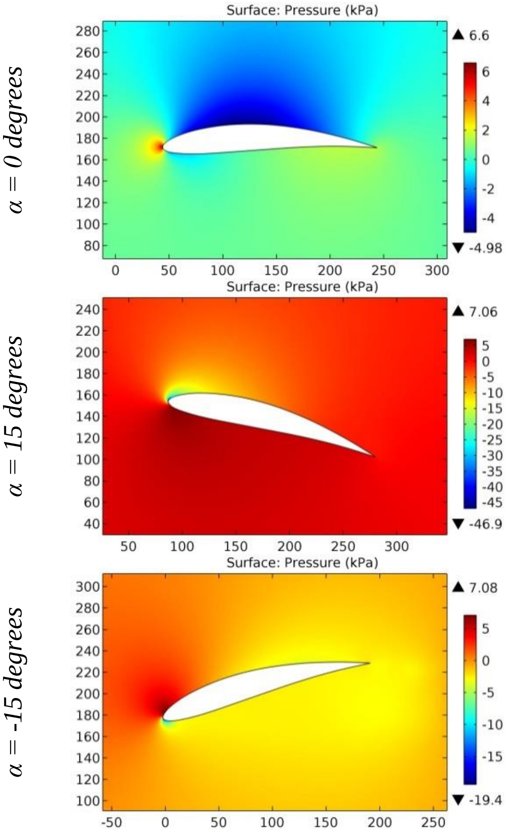

Figure 19. The pressure contours on the surfaces of the RAF 32 airfoil.

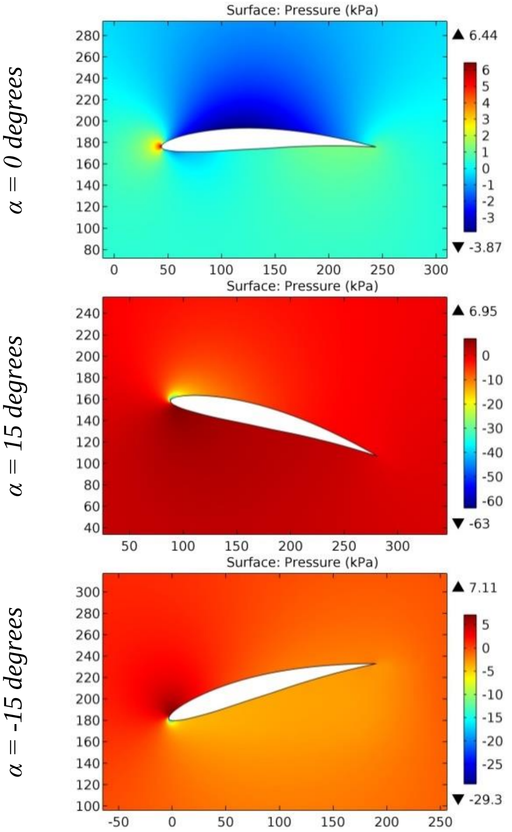

Figure 20. The pressure contours on the surfaces of the RAF 32 MOD airfoil.

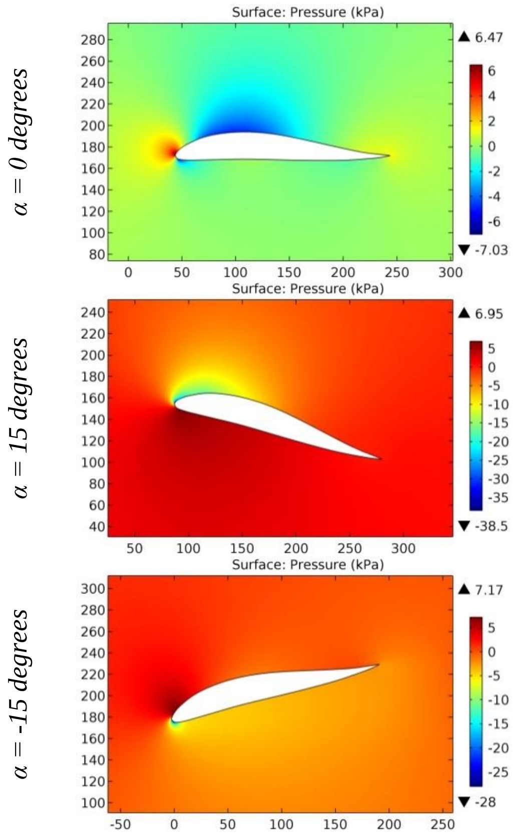

Figure 21. The pressure contours on the surfaces of the RAF 33 airfoil.

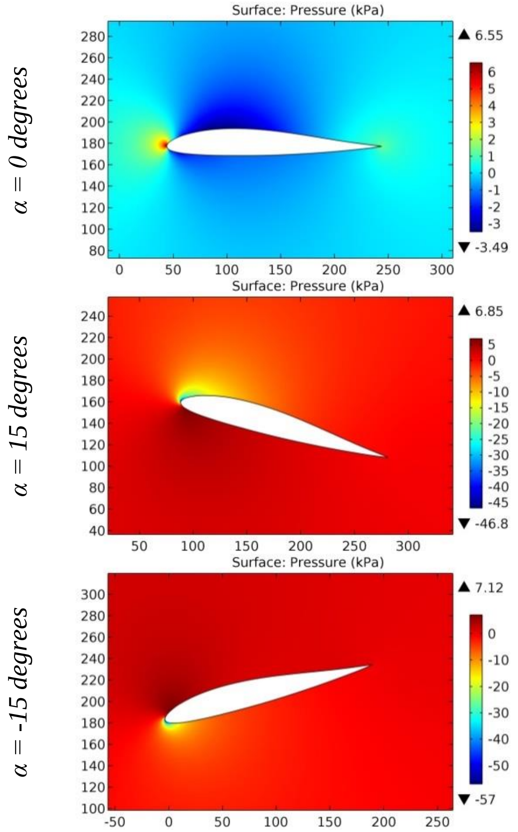

Figure 22. The pressure contours on the surfaces of the RAF 34 airfoil.

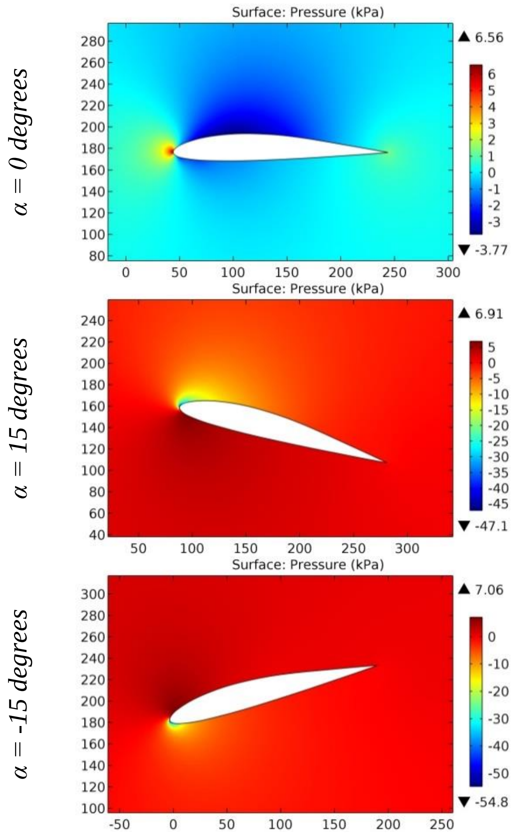

Figure 23. The pressure contours on the surfaces of the RAF 38 airfoil.

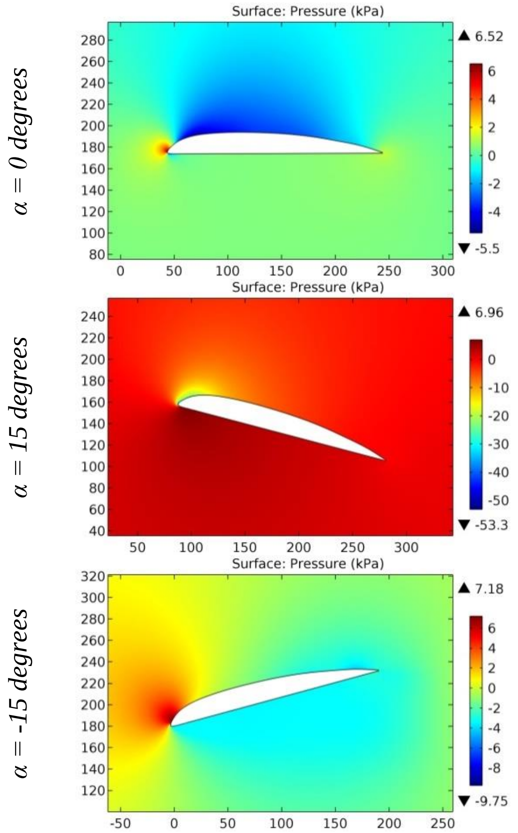

Figure 24. The pressure contours on the surfaces of the RAF 6 airfoil.

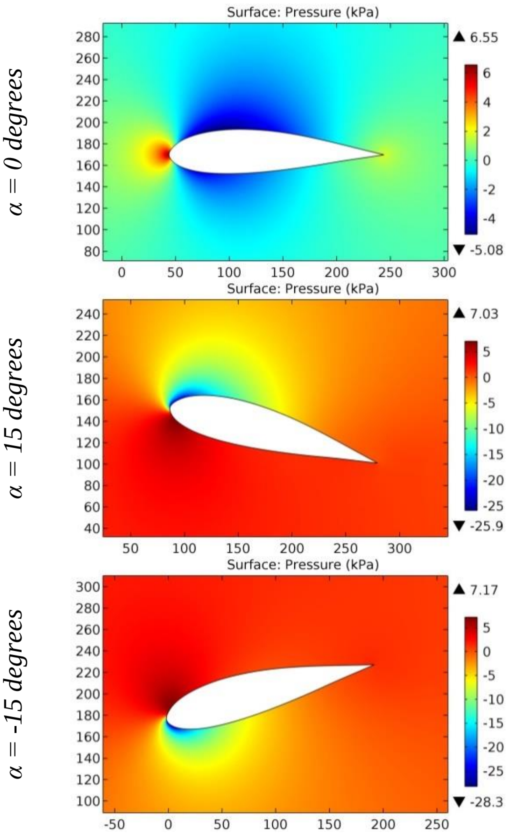

Figure 25. The pressure contours on the surfaces of the RAF 69 airfoil.

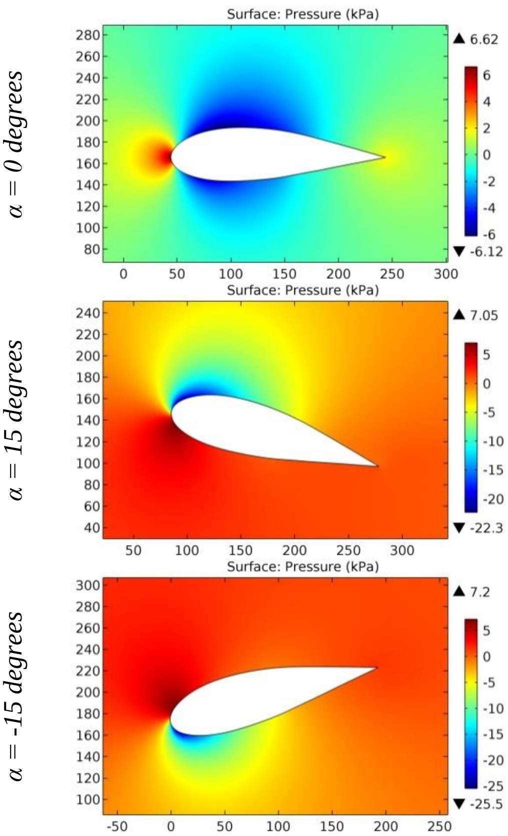

Figure 26. The pressure contours on the surfaces of the RAF 89 airfoil.

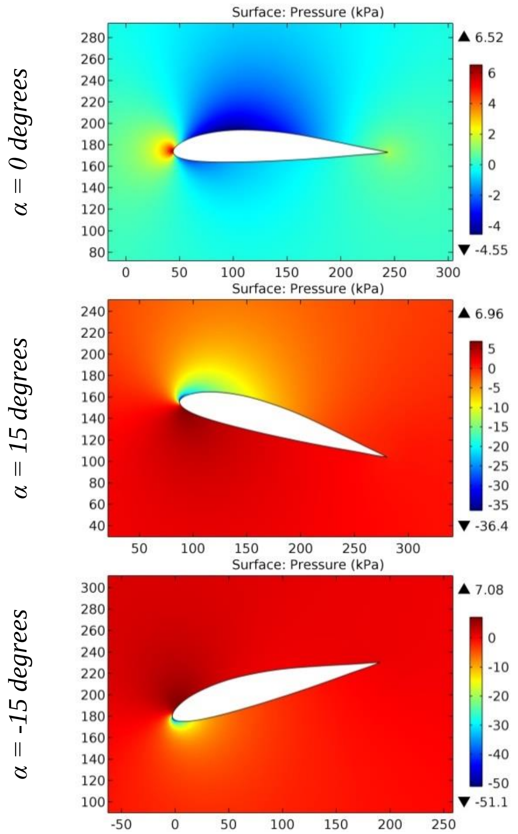

Figure 27. The pressure contours on the surfaces of the RAF-48 airfoil.

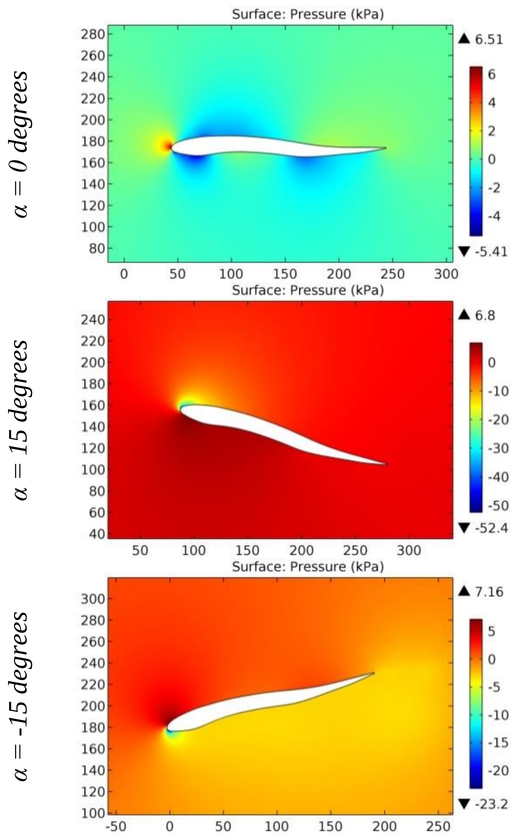

Figure 28. The pressure contours on the surfaces of the REFLEXS1 airfoil.

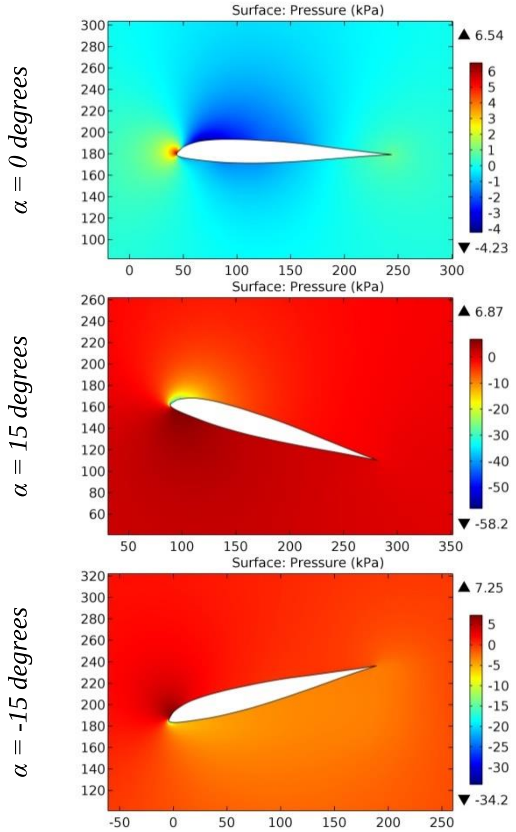

Figure 29. The pressure contours on the surfaces of the REPUBLIC S-3 airfoil.

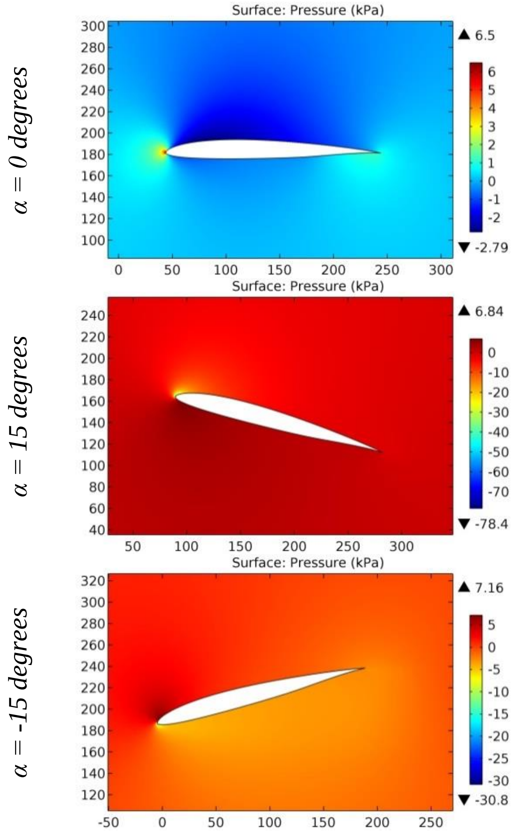

Figure 30. The pressure contours on the surfaces of the RG 12A-1,8-9,0 airfoil.

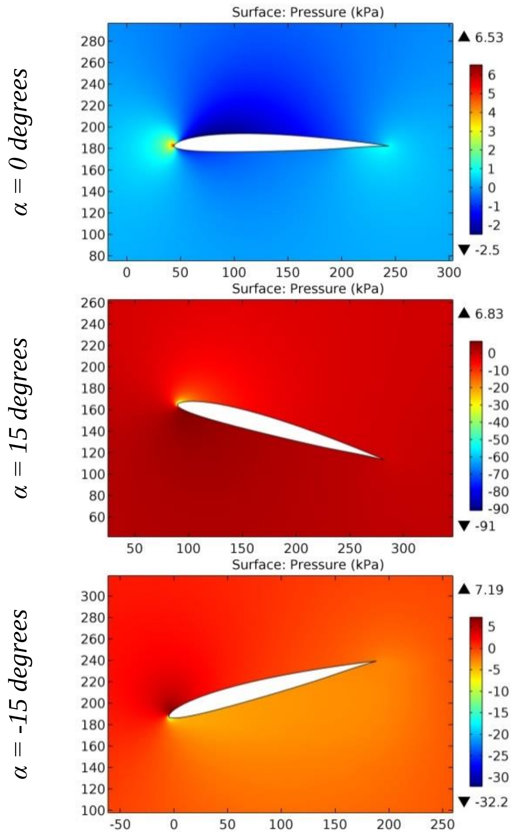

Figure 31. The pressure contours on the surfaces of the RG 14 airfoil.

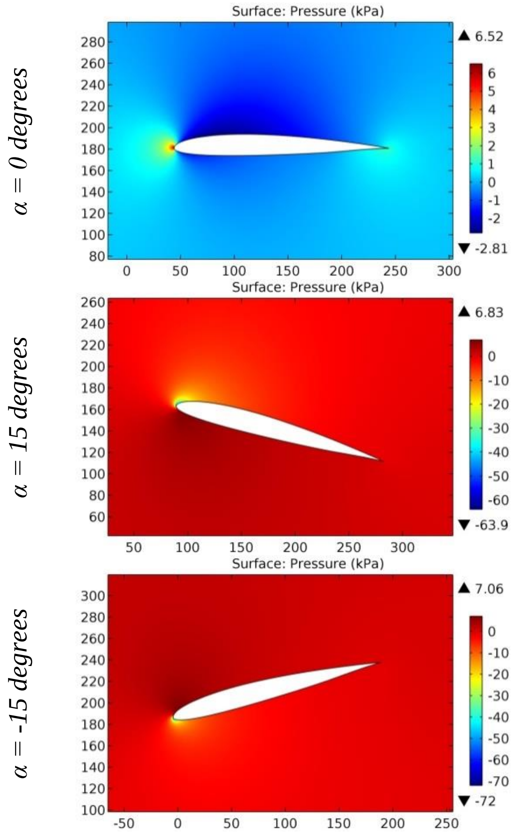

Figure 32. The pressure contours on the surfaces of the RG 14 10% airfoil.

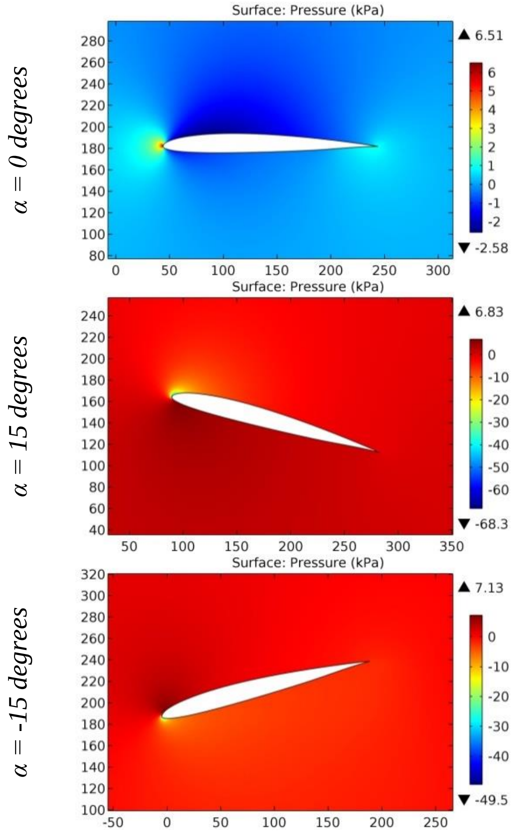

Figure 33. The pressure contours on the surfaces of the RG 14 9% airfoil.

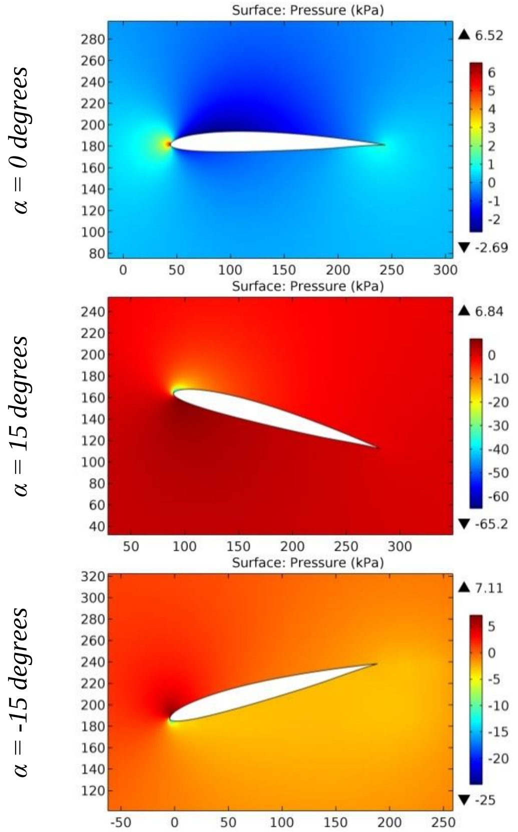

Figure 34. The pressure contours on the surfaces of the RG 14 9,5% airfoil.

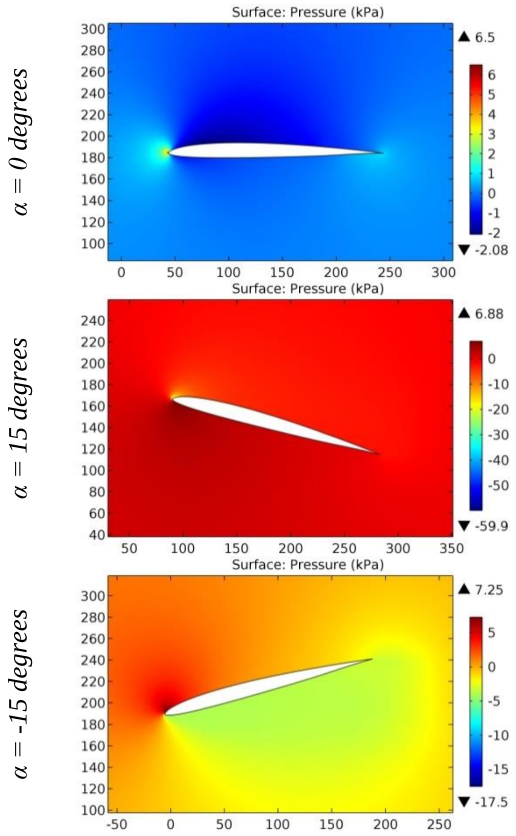

Figure 35. The pressure contours on the surfaces of the RG 14A-1,4-7,0 airfoil.

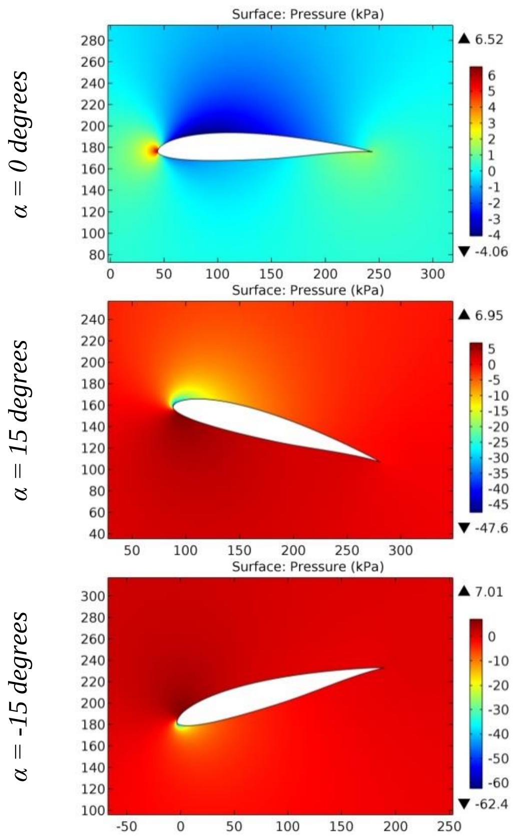

Figure 36. The pressure contours on the surfaces of the RG 15A 2,5-13,0 airfoil.

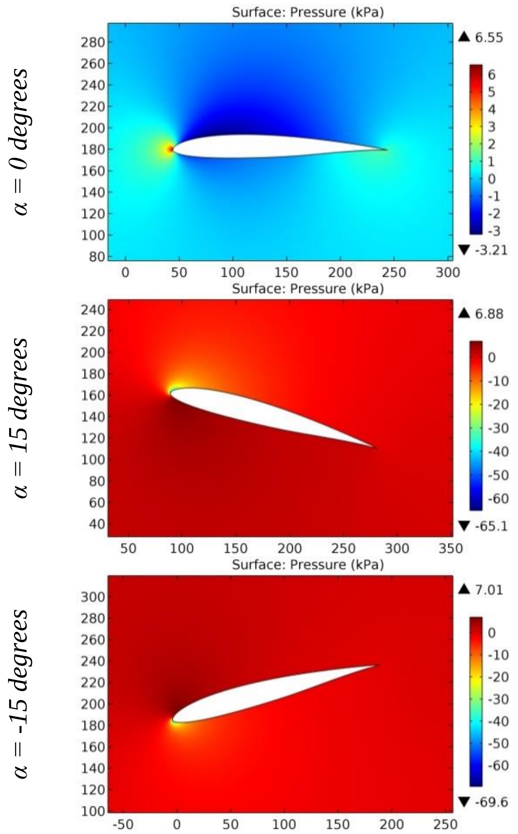

Figure 37. The pressure contours on the surfaces of the RG 15A-1,8-11,0 airfoil.

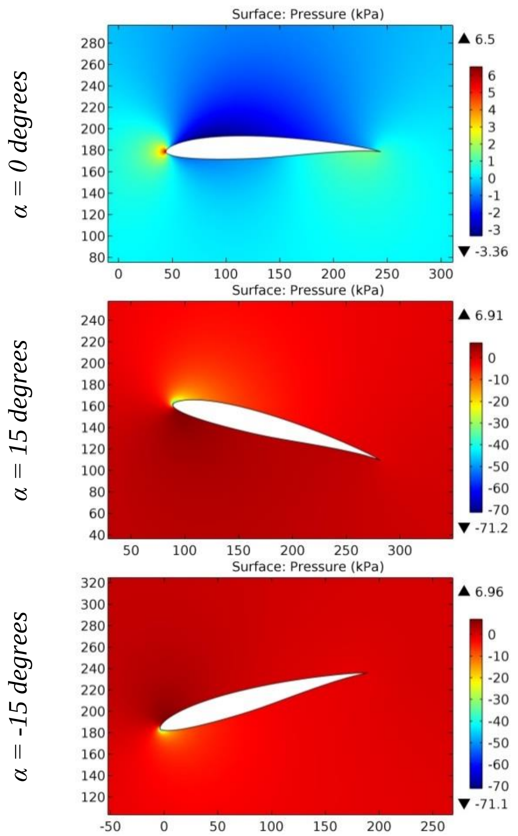

Figure 38. The pressure contours on the surfaces of the RG 8 airfoil.

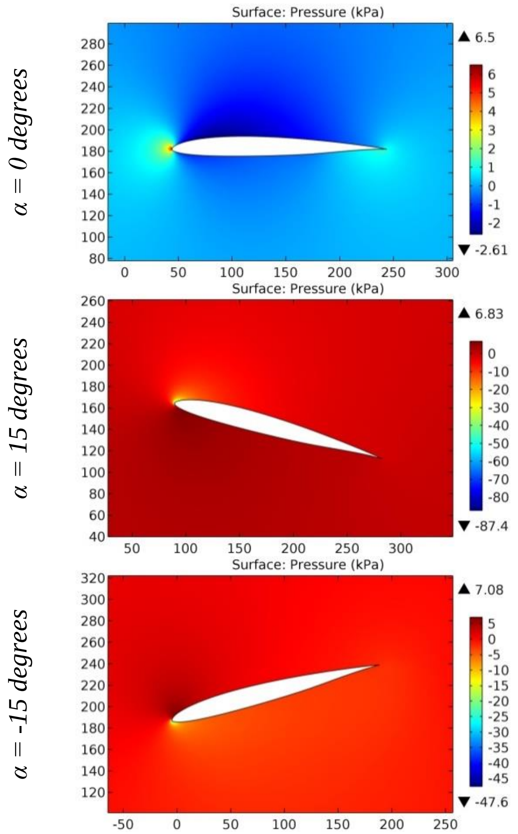

Figure 39. The pressure contours on the surfaces of the RG-12 airfoil.

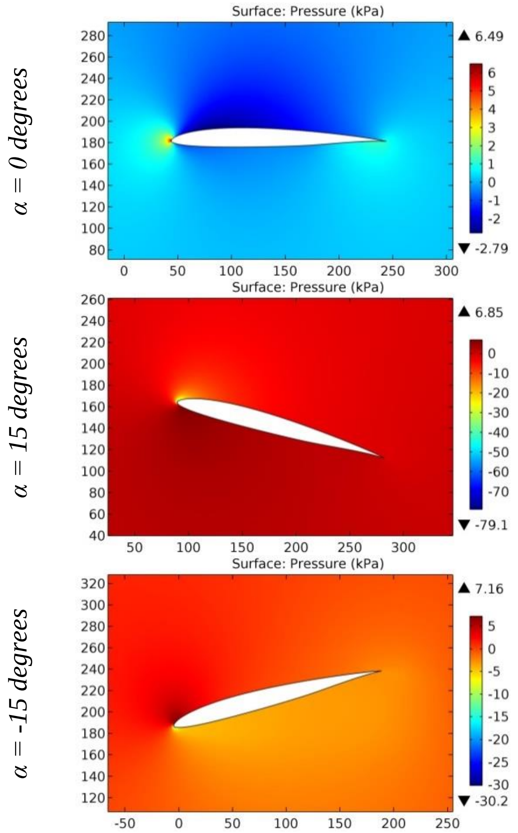

Figure 40. The pressure contours on the surfaces of the RG-12A airfoil.

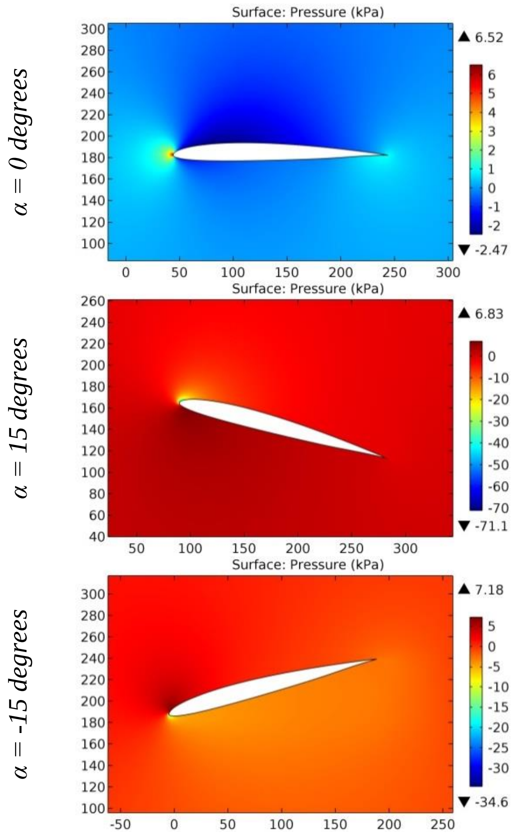

Figure 41. The pressure contours on the surfaces of the RG-14 airfoil.

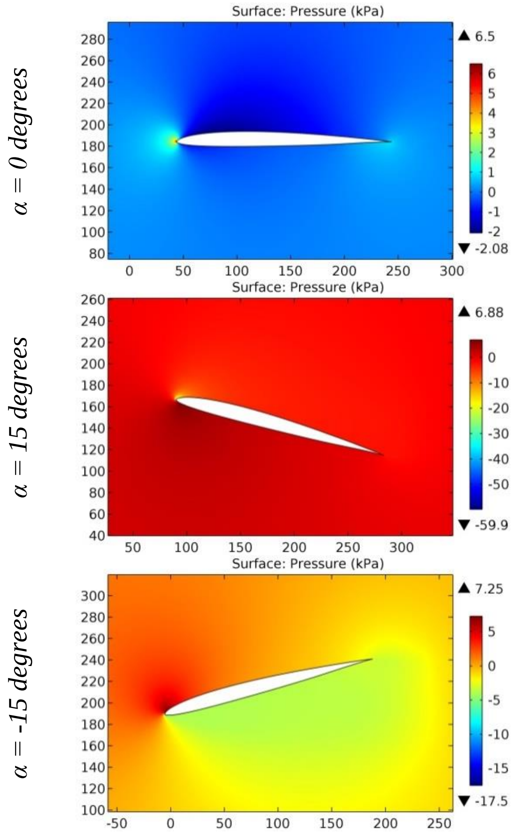

Figure 42. The pressure contours on the surfaces of the RG14A147 airfoil.

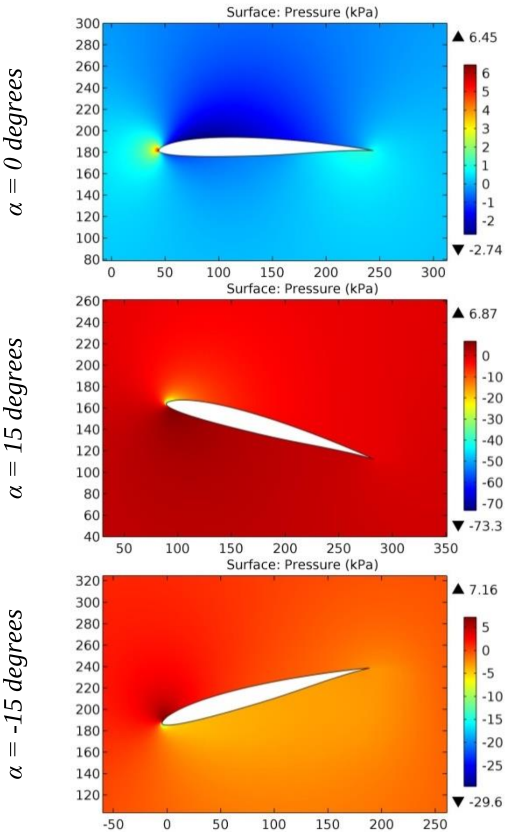

Figure 43. The pressure contours on the surfaces of the RG-15 airfoil.

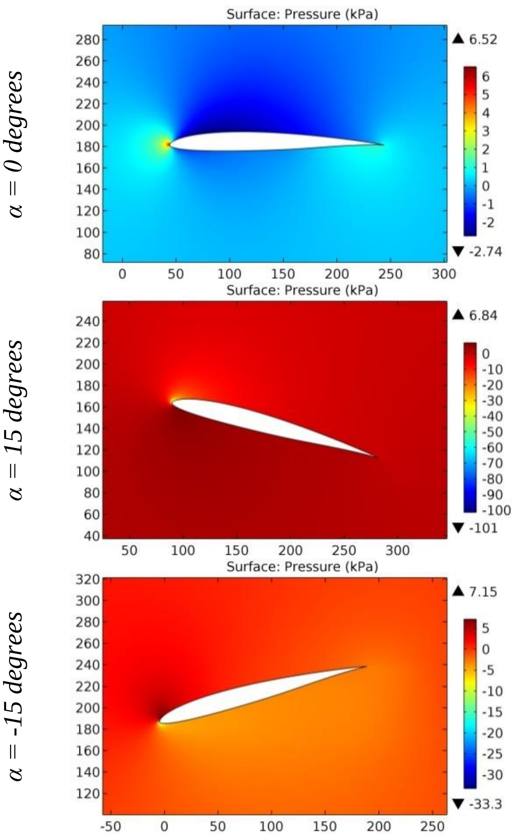

Figure 44. The pressure contours on the surfaces of the RG-15 8,9% airfoil.

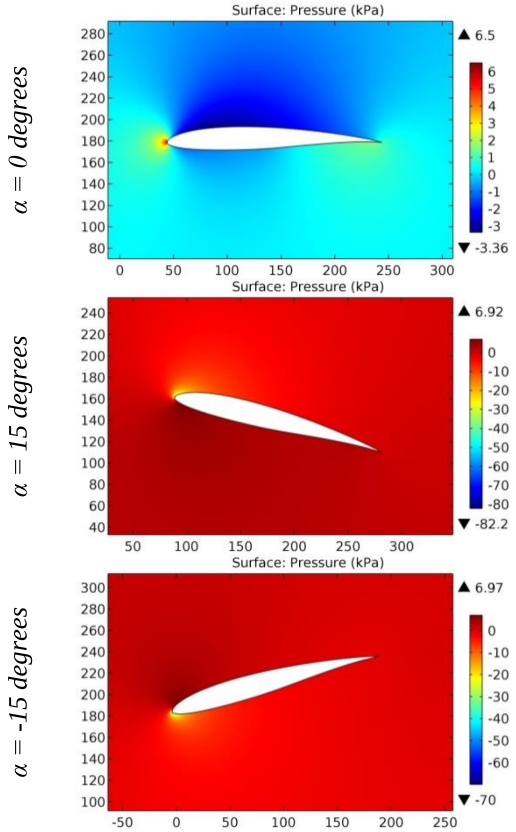

Figure 45. The pressure contours on the surfaces of the RG-8 airfoil.

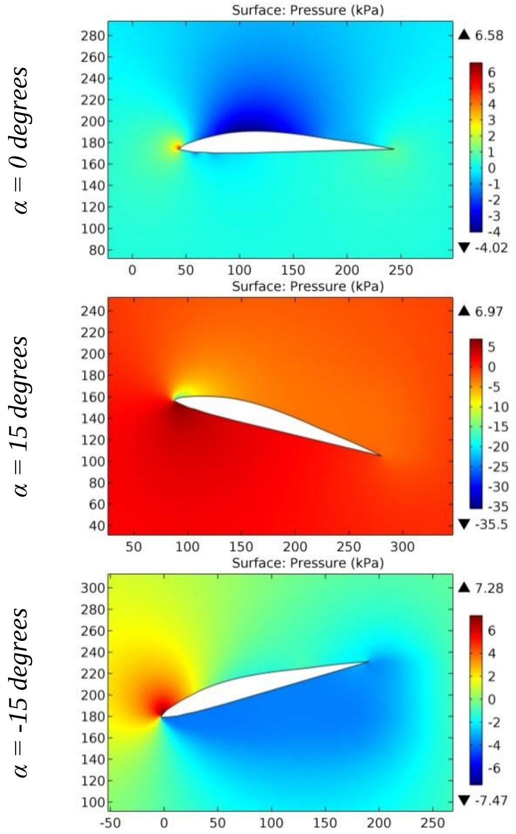

Figure 46. The pressure contours on the surfaces of the Rhode St Genese 26 airfoil.

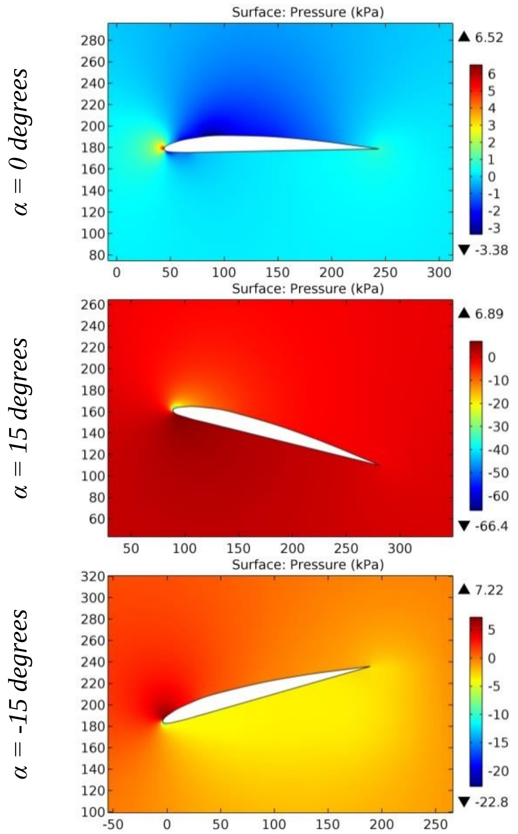

Figure 47. The pressure contours on the surfaces of the Rhode St Genese 28 airfoil.

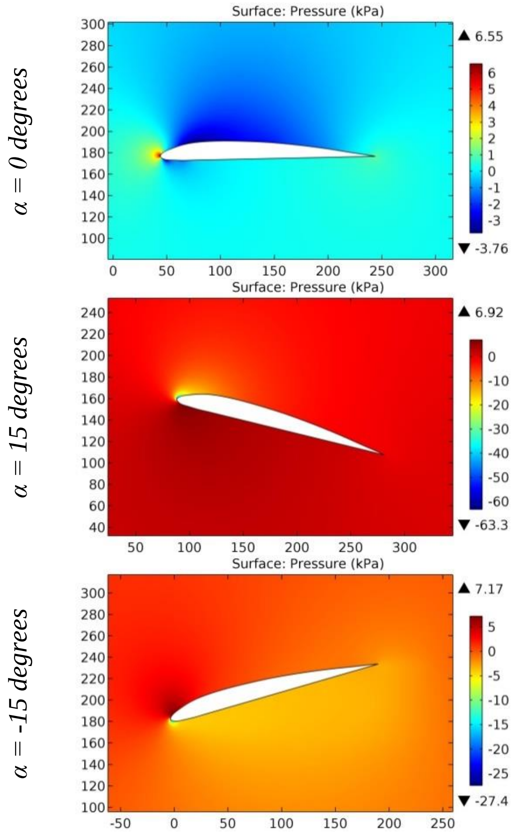

Figure 48. The pressure contours on the surfaces of the Rhode St Genese 29 airfoil.

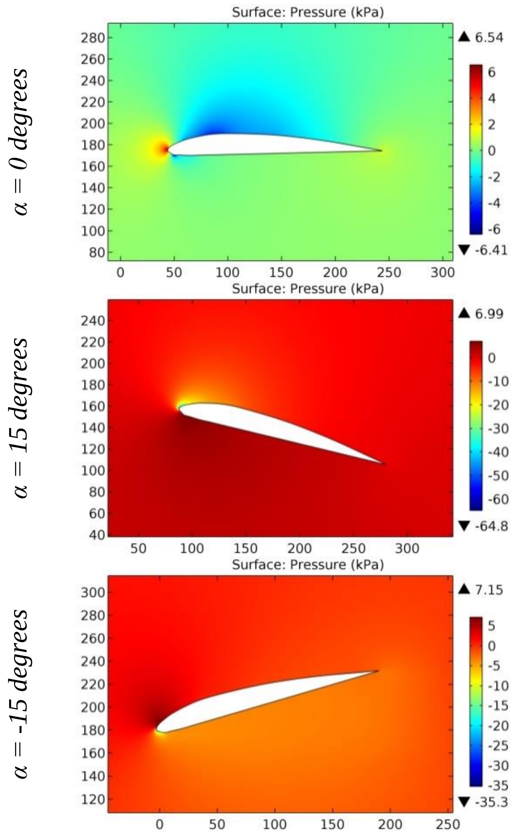

Figure 49. The pressure contours on the surfaces of the Rhode St Genese 30 airfoil.

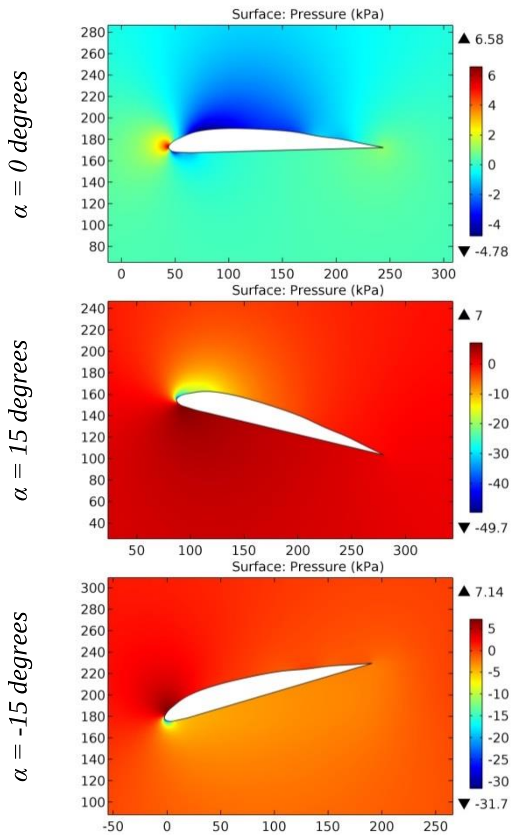

Figure 50. The pressure contours on the surfaces of the Rhode St Genese 31 airfoil.

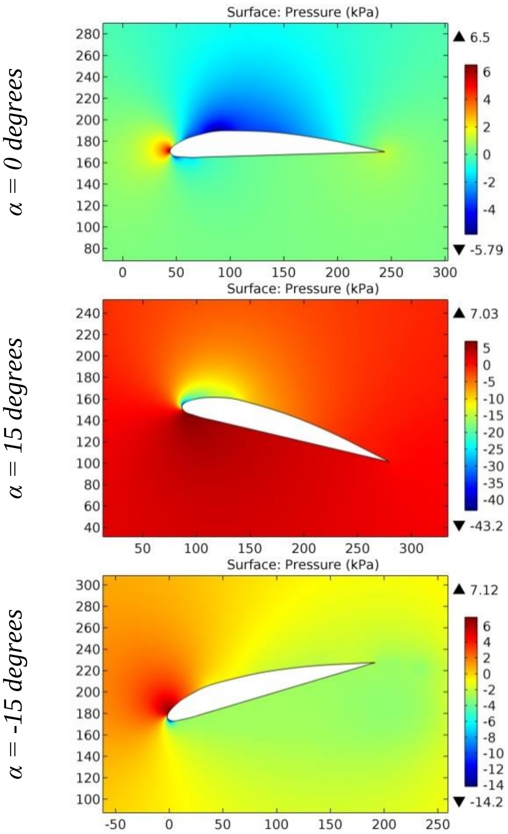

Figure 51. The pressure contours on the surfaces of the Rhode St Genese 32 airfoil.

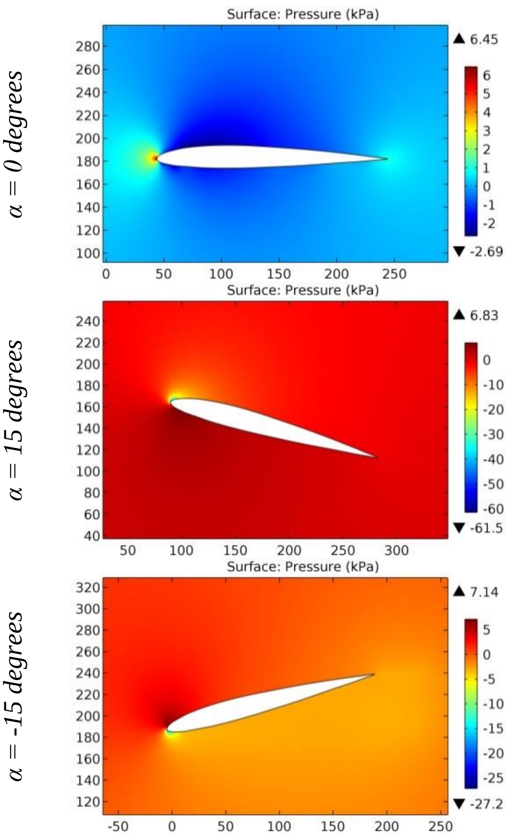

Figure 52. The pressure contours on the surfaces of the Ritz 1-30-10 airfoil.

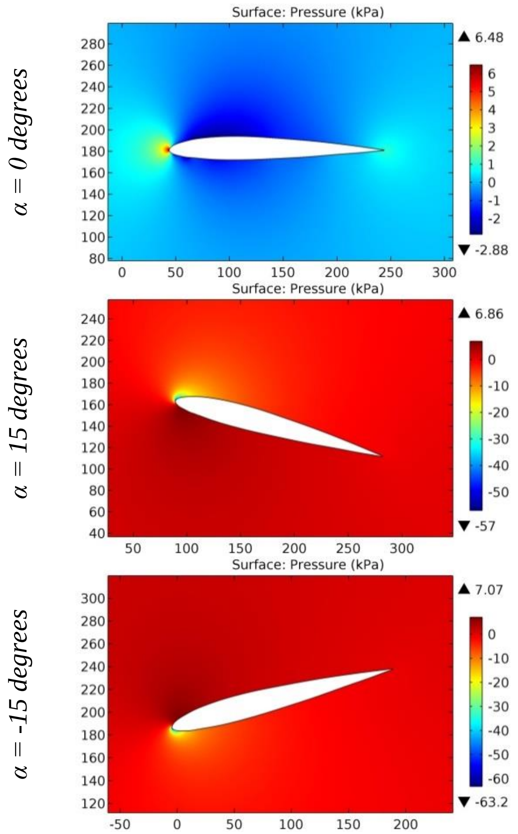

Figure 53. The pressure contours on the surfaces of the Ritz 1-30-11 airfoil.

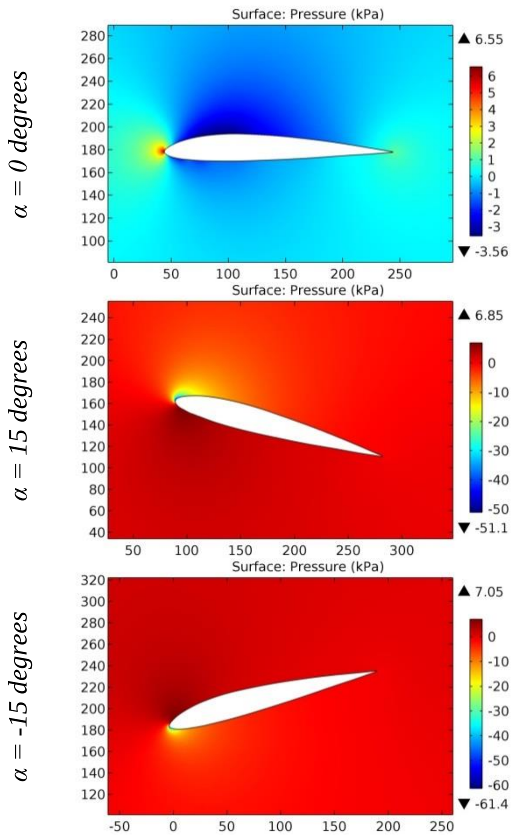

Figure 54. The pressure contours on the surfaces of the Ritz 1-30-12 airfoil.

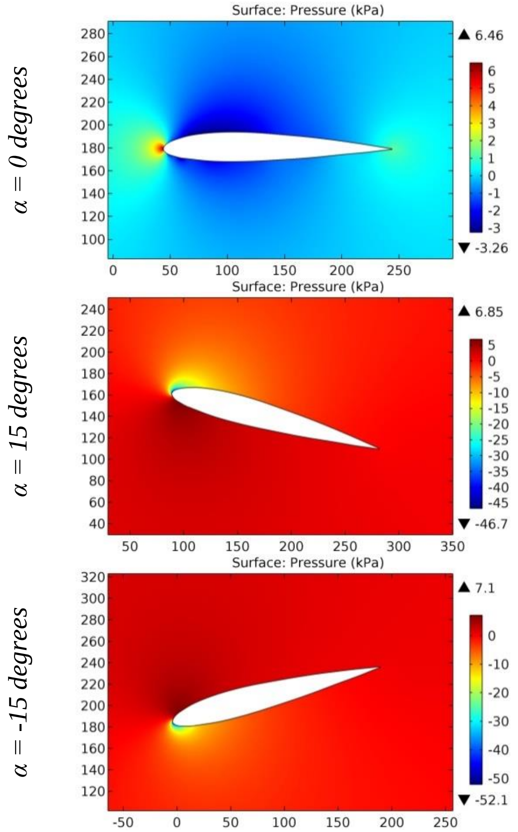

Figure 55. The pressure contours on the surfaces of the Ritz 1-30-13 airfoil.

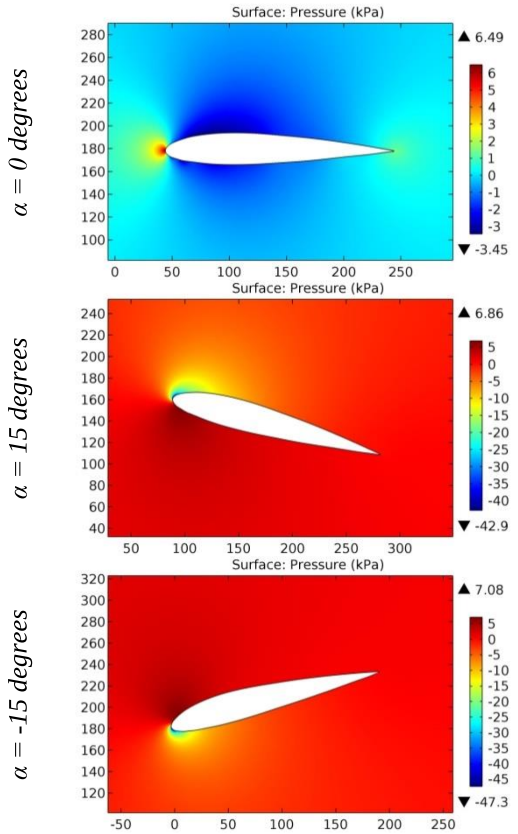

Figure 56. The pressure contours on the surfaces of the Ritz 1-30-14 airfoil.

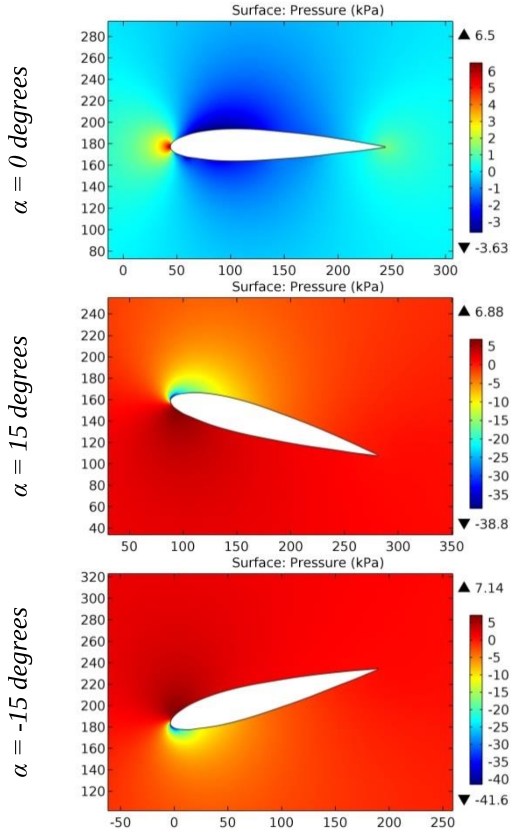

Figure 57. The pressure contours on the surfaces of the Ritz 1-30-15 airfoil.

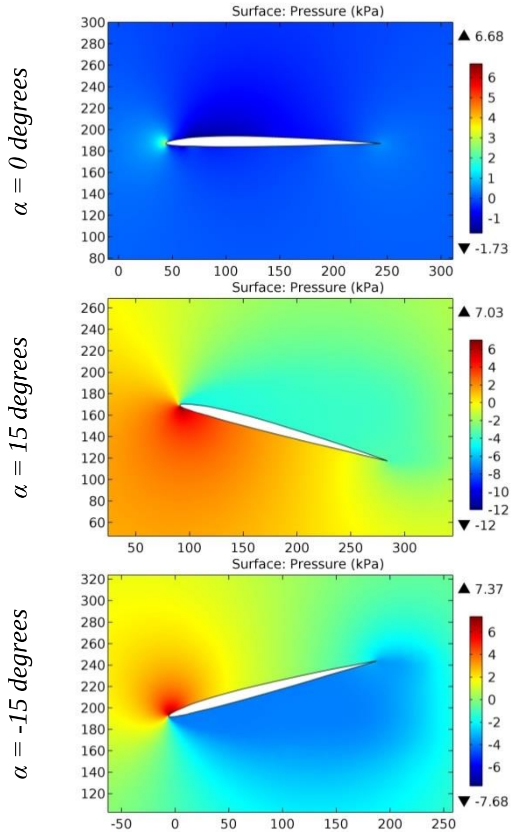

Figure 58. The pressure contours on the surfaces of the Ritz 1-30-5 airfoil.

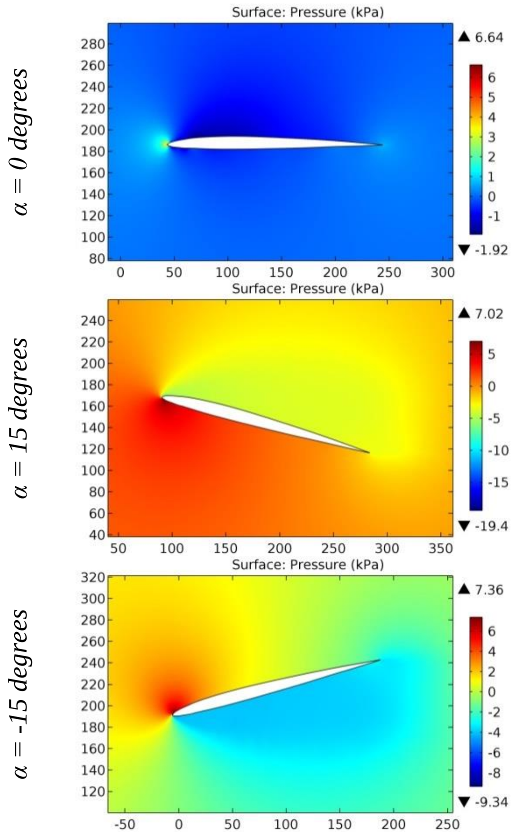

Figure 59. The pressure contours on the surfaces of the Ritz 1-30-6 airfoil.

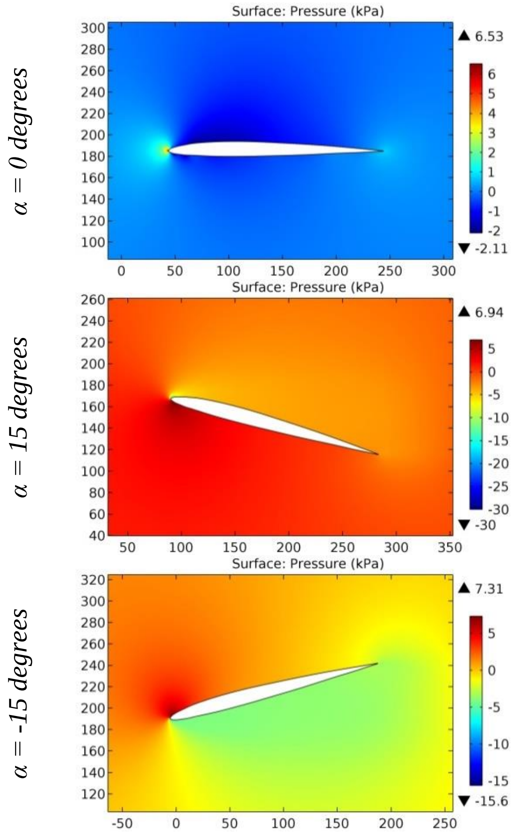

Figure 60. The pressure contours on the surfaces of the Ritz 1-30-7 airfoil.

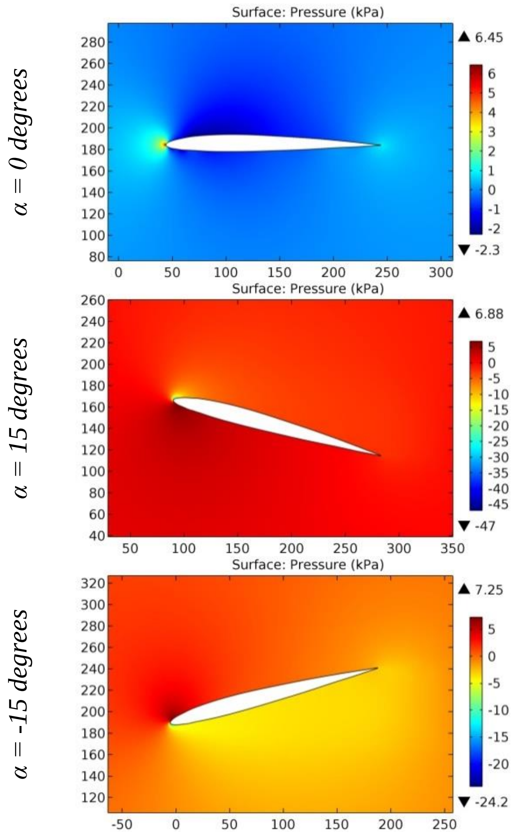

Figure 61. The pressure contours on the surfaces of the Ritz 1-30-8 airfoil.

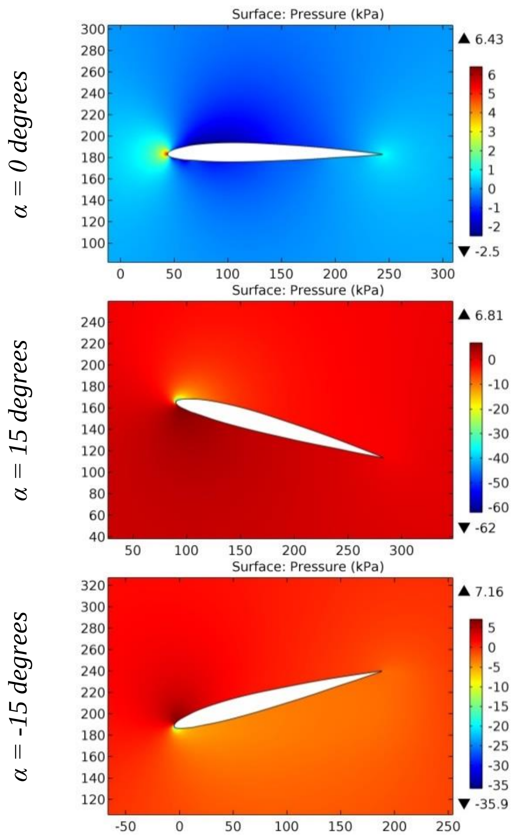

Figure 62. The pressure contours on the surfaces of the Ritz 1-30-9 airfoil.

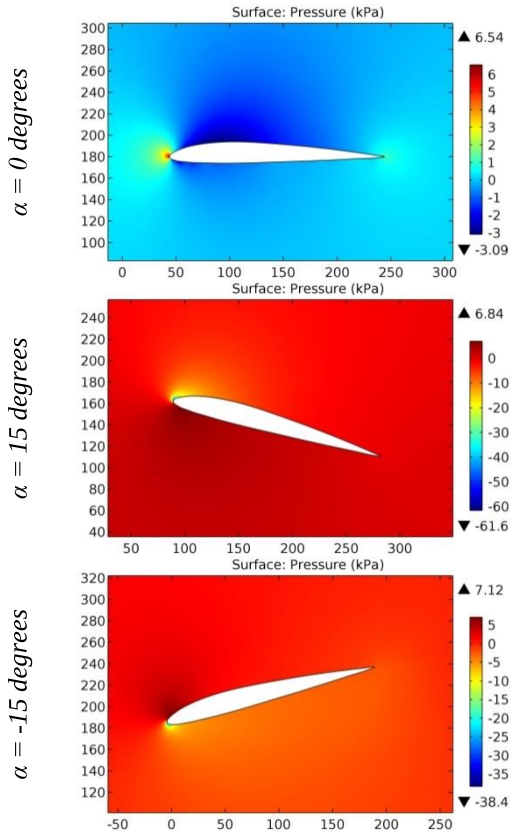

Figure 63. The pressure contours on the surfaces of the Ritz 2-30-10 airfoil.

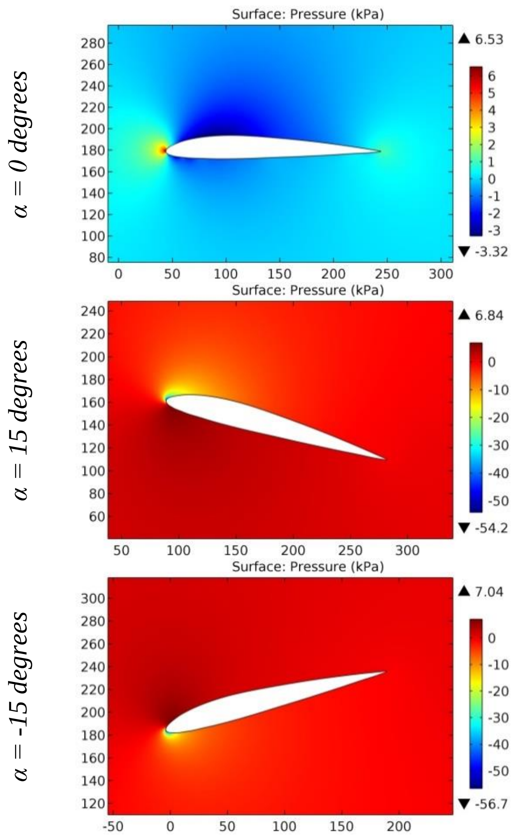

Figure 64. The pressure contours on the surfaces of the Ritz 2-30-11 airfoil.

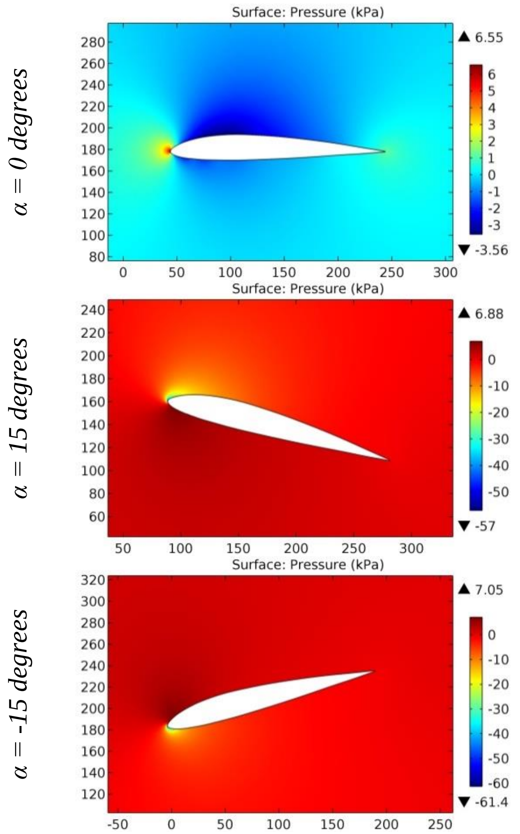

Figure 65. The pressure contours on the surfaces of the Ritz 2-30-12 airfoil.

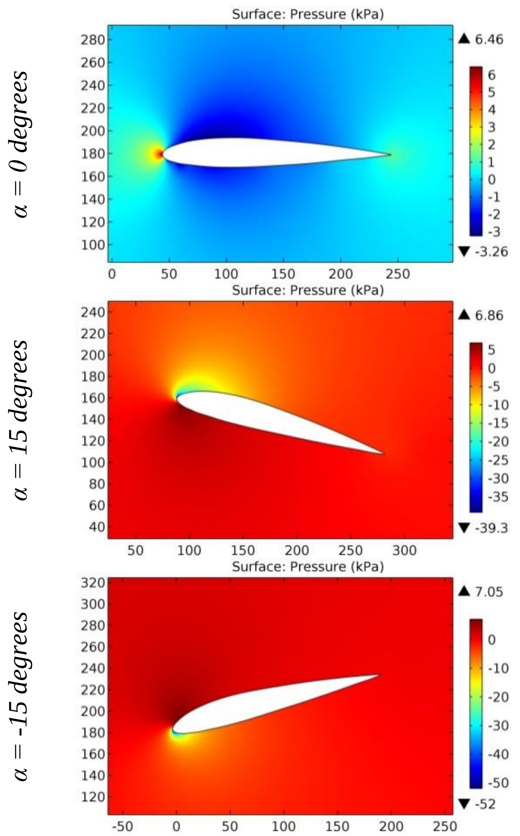

Figure 66. The pressure contours on the surfaces of the Ritz 2-30-13 airfoil.

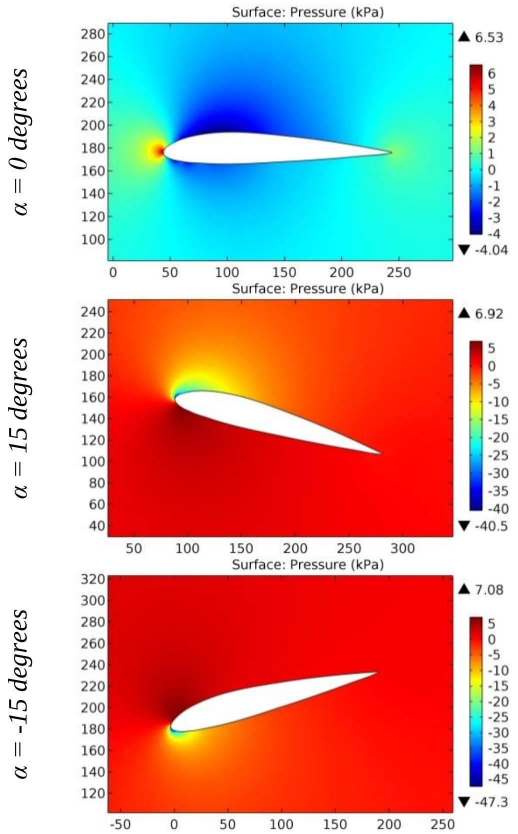

Figure 67. The pressure contours on the surfaces of the Ritz 2-30-14 airfoil.

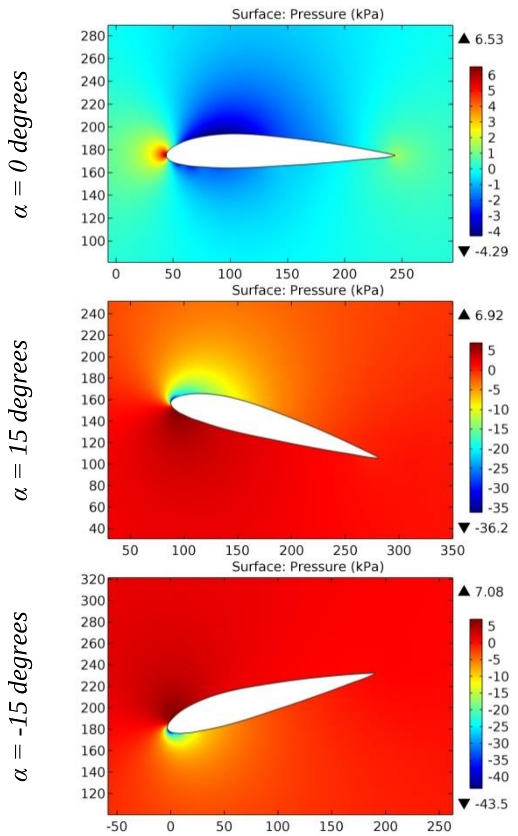

Figure 68. The pressure contours on the surfaces of the Ritz 2-30-15 airfoil.

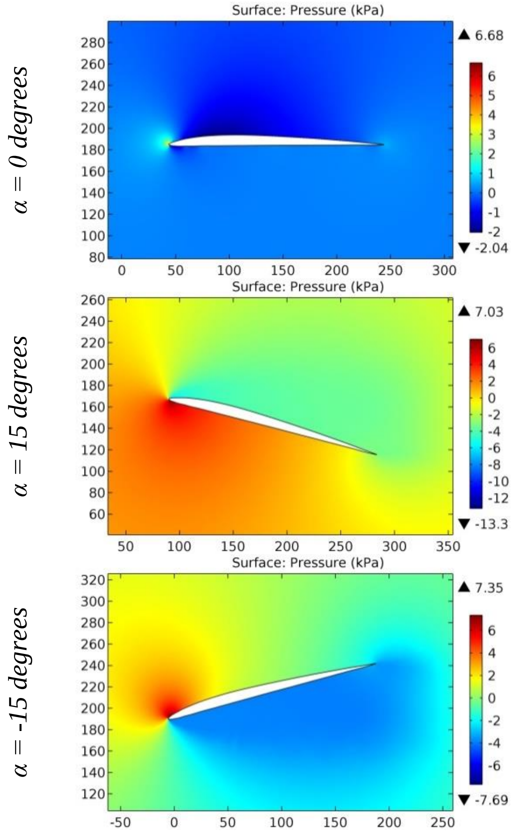

Figure 69. The pressure contours on the surfaces of the Ritz 2-30-5 airfoil.

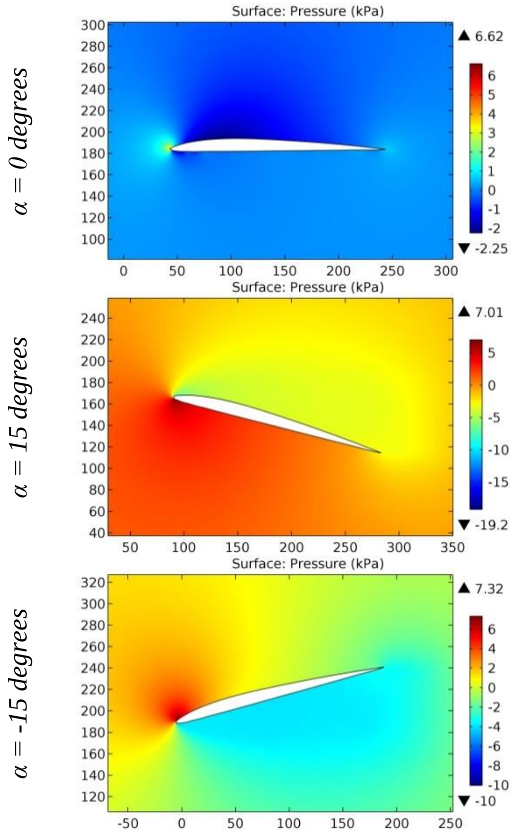

Figure 70. The pressure contours on the surfaces of the Ritz 2-30-6 airfoil.

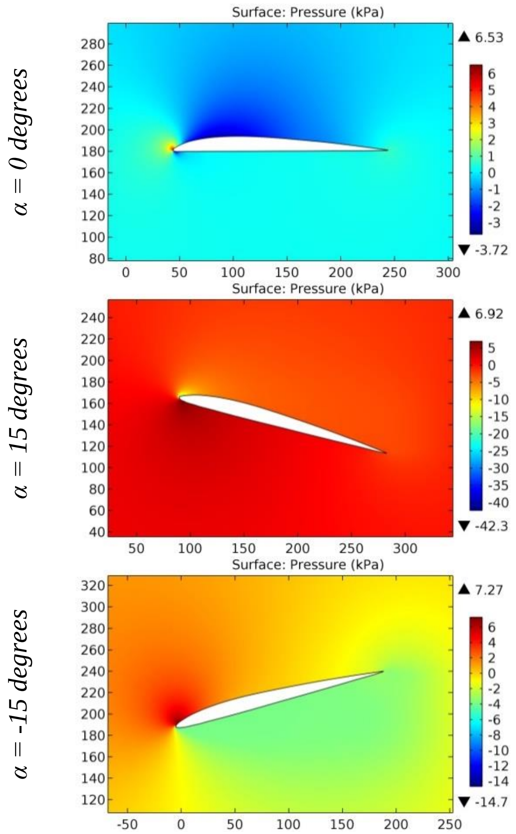

Figure 71. The pressure contours on the surfaces of the Ritz 2-30-7 airfoil.

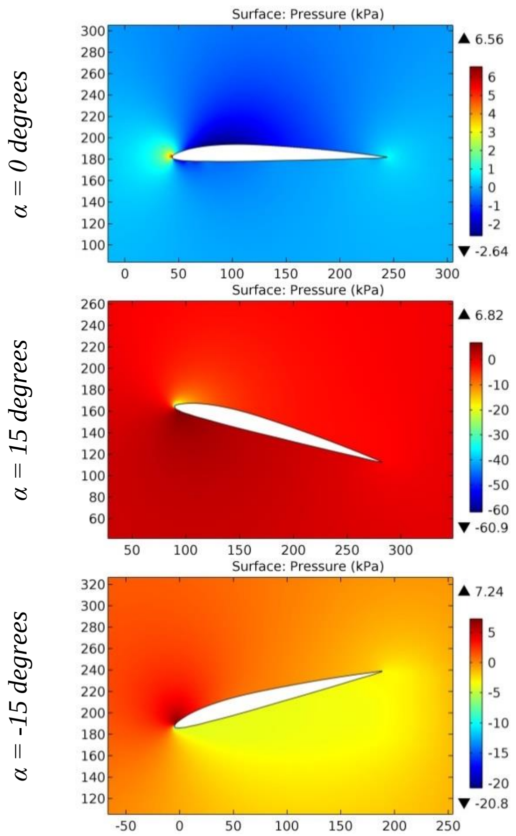

Figure 72. The pressure contours on the surfaces of the Ritz 2-30-8 airfoil.

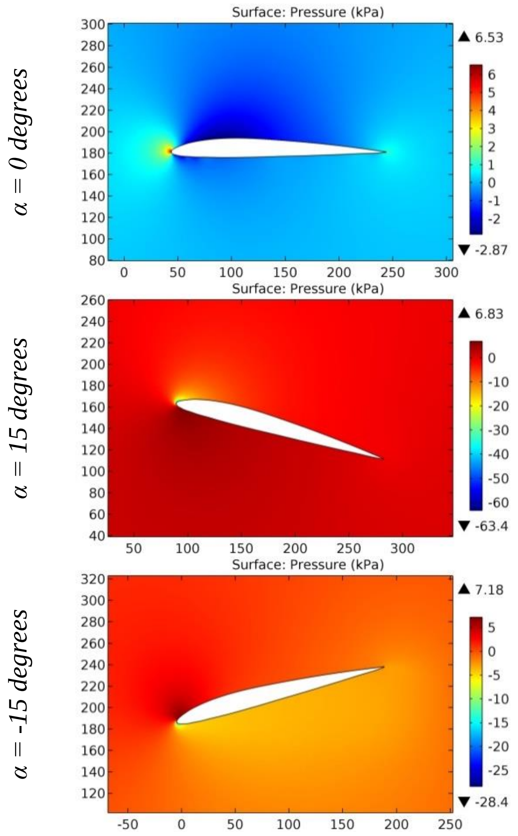

Figure 73. The pressure contours on the surfaces of the Ritz 2-30-9 airfoil.

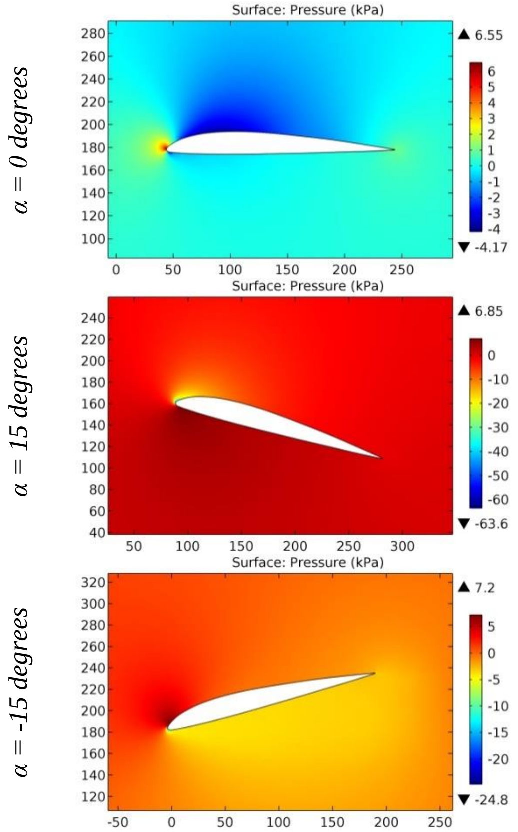

Figure 74. The pressure contours on the surfaces of the Ritz 3-30-10 airfoil.

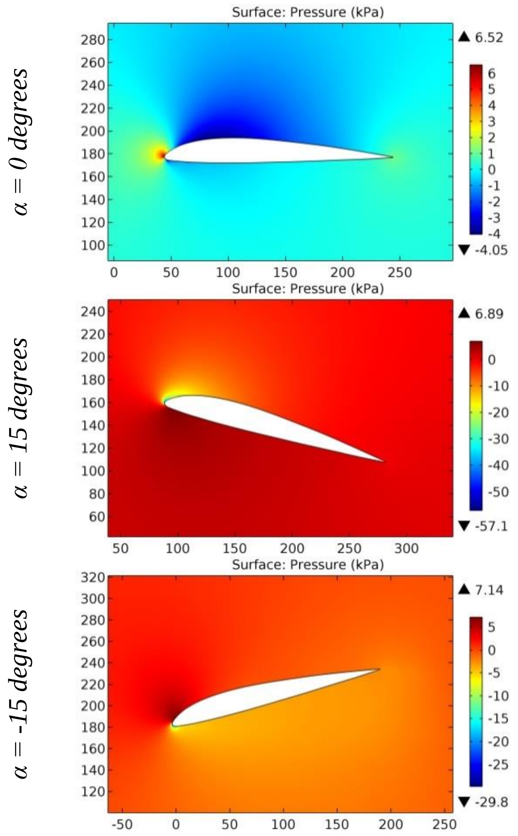

Figure 75. The pressure contours on the surfaces of the Ritz 3-30-11 airfoil.

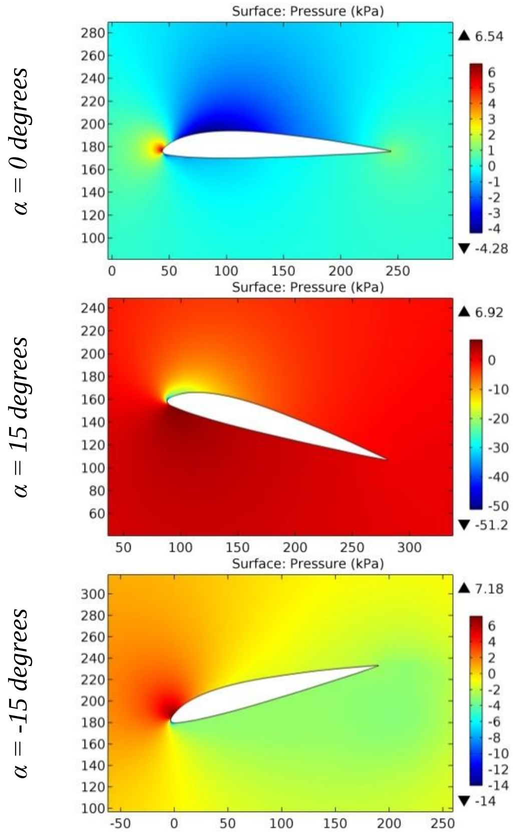

Figure 76. The pressure contours on the surfaces of the Ritz 3-30-12 airfoil.

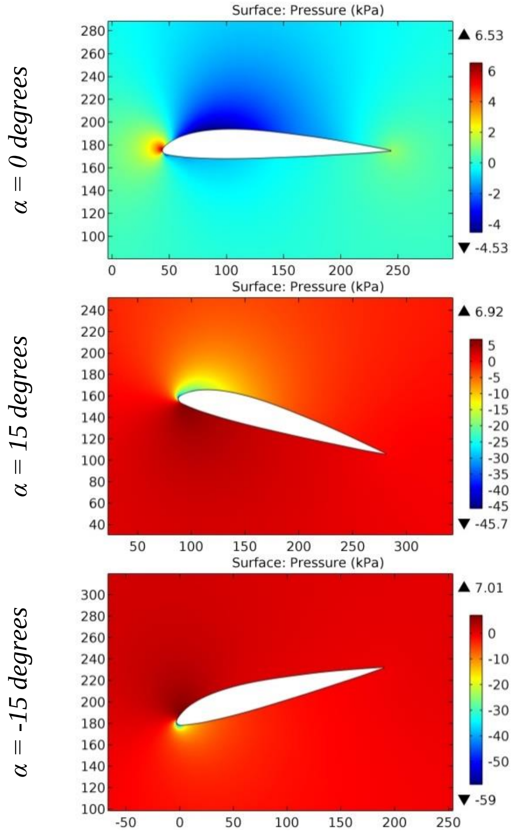

Figure 77. The pressure contours on the surfaces of the Ritz 3-30-13 airfoil.

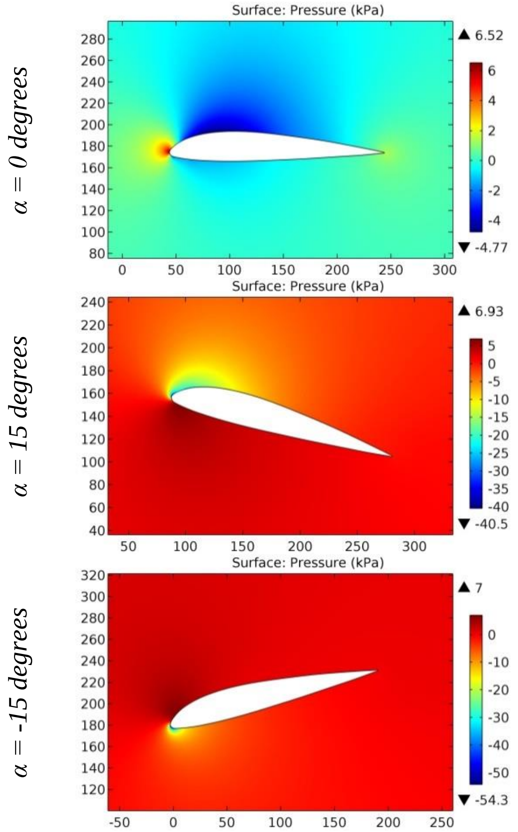

Figure 78. The pressure contours on the surfaces of the Ritz 3-30-14 airfoil.

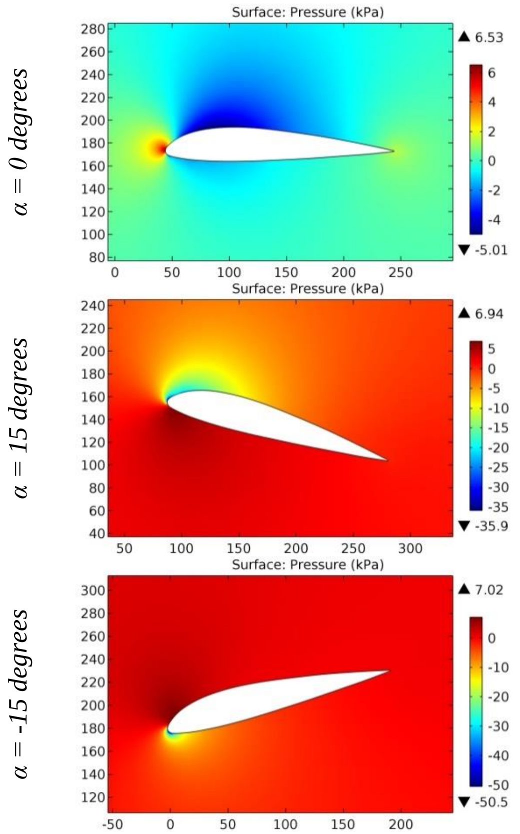

Figure 79. The pressure contours on the surfaces of the Ritz 3-30-15 airfoil.

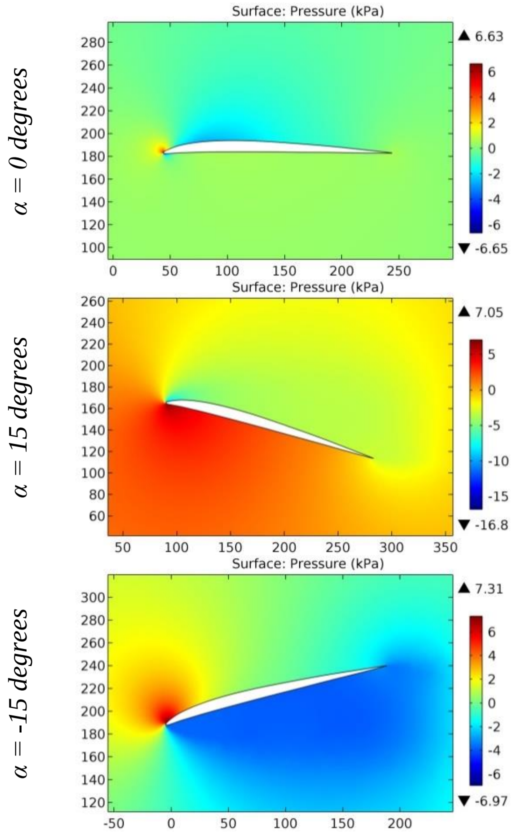

Figure 80. The pressure contours on the surfaces of the Ritz 3-30-5 airfoil.

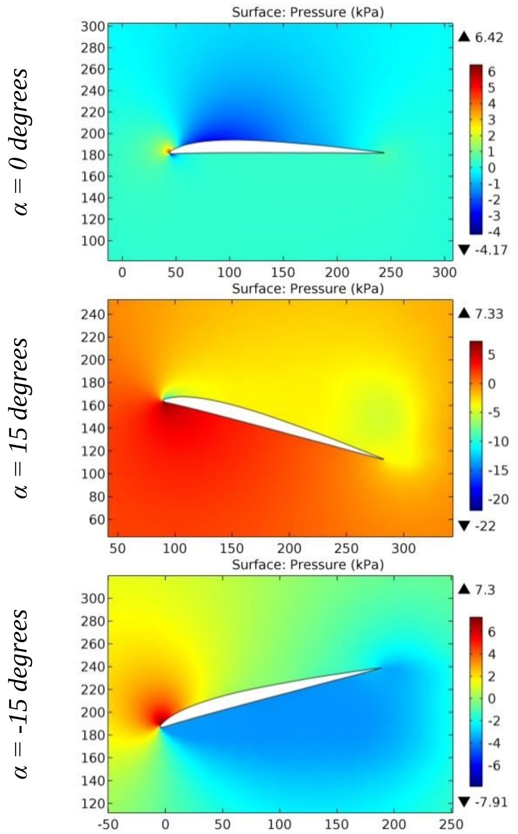

Figure 81. The pressure contours on the surfaces of the Ritz 3-30-6 airfoil.

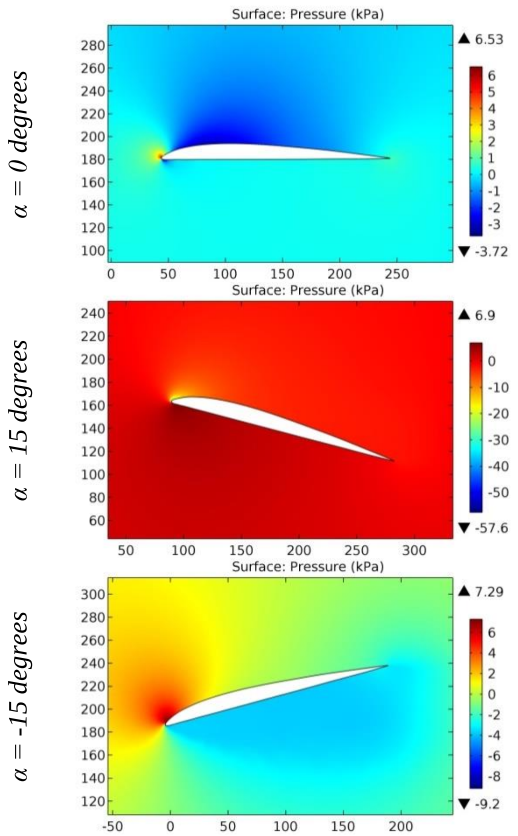

Figure 82. The pressure contours on the surfaces of the Ritz 3-30-7 airfoil.

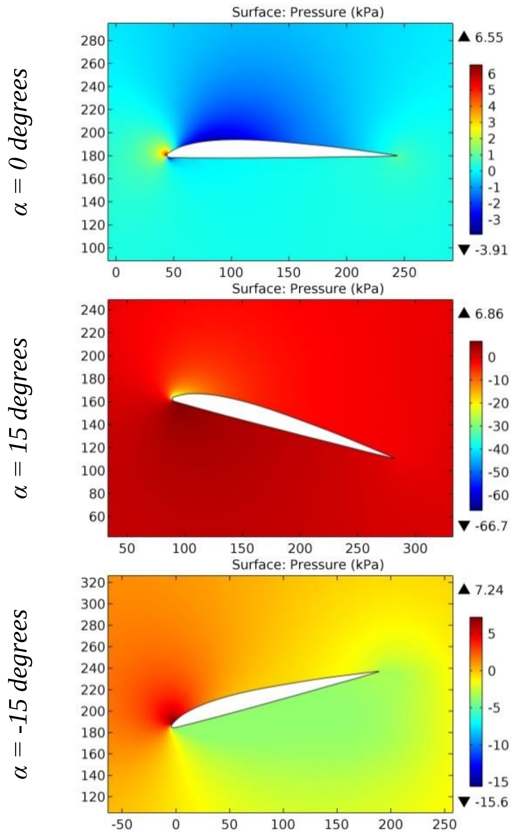

Figure 83. The pressure contours on the surfaces of the Ritz 3-30-8 airfoil.

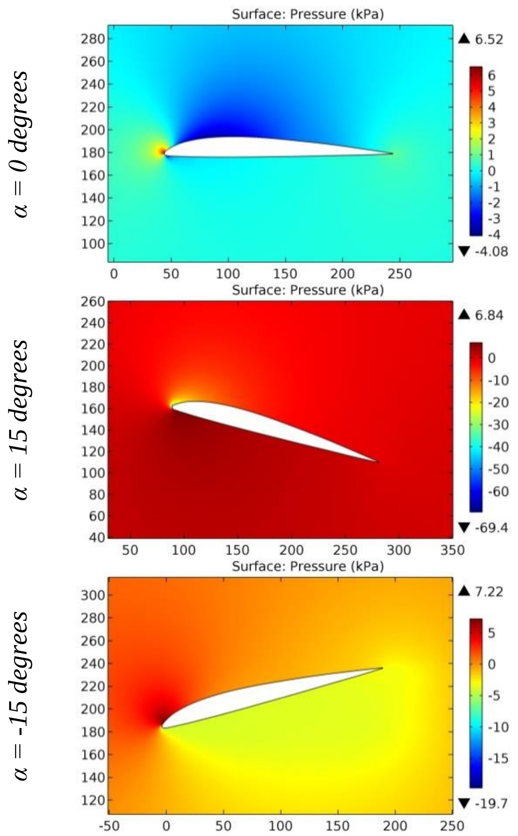

Figure 84. The pressure contours on the surfaces of the Ritz 3-30-9 airfoil.

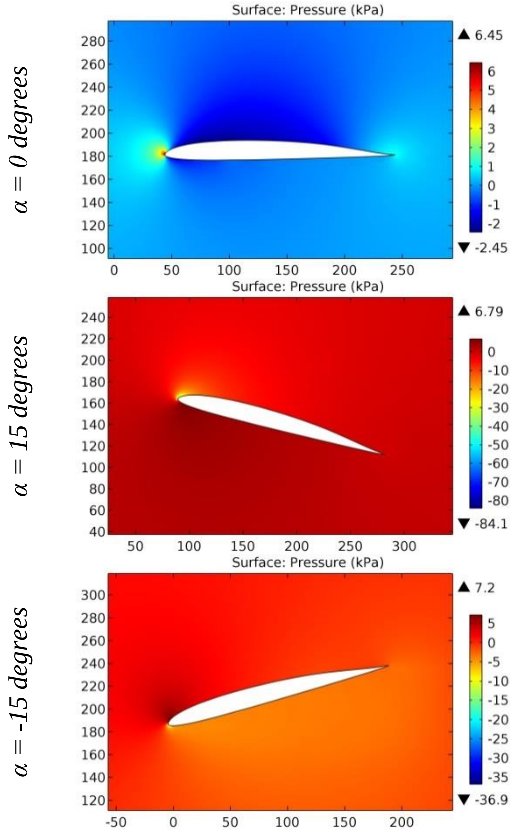

Figure 85. The pressure contours on the surfaces of the RK40 airfoil.

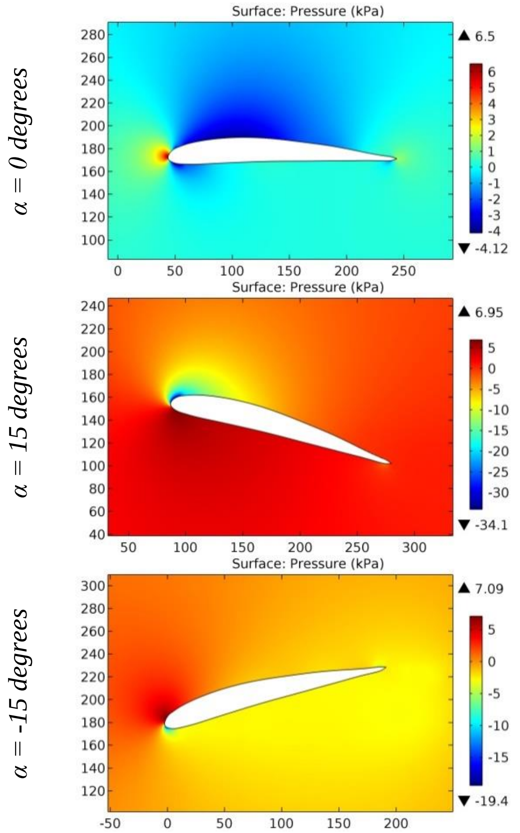

Figure 86. The pressure contours on the surfaces of the Roma 701 airfoil.

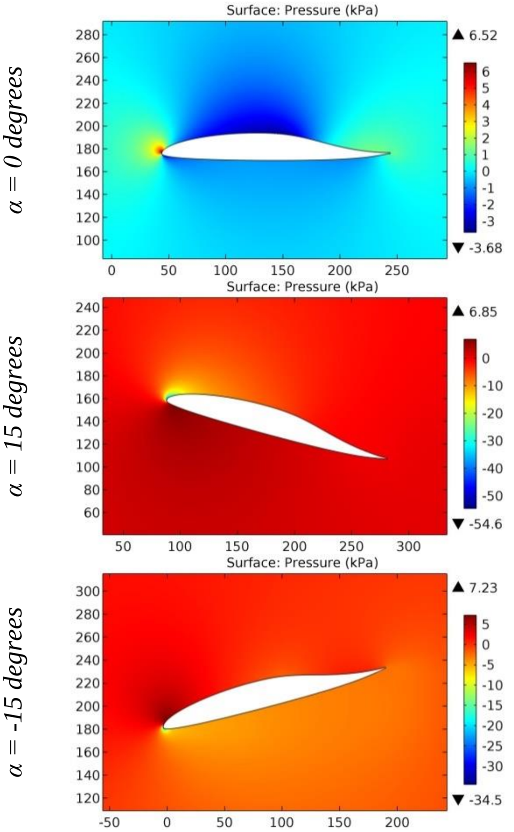

Figure 87. The pressure contours on the surfaces of the RONCZ LOW DRAG FLYING WING.

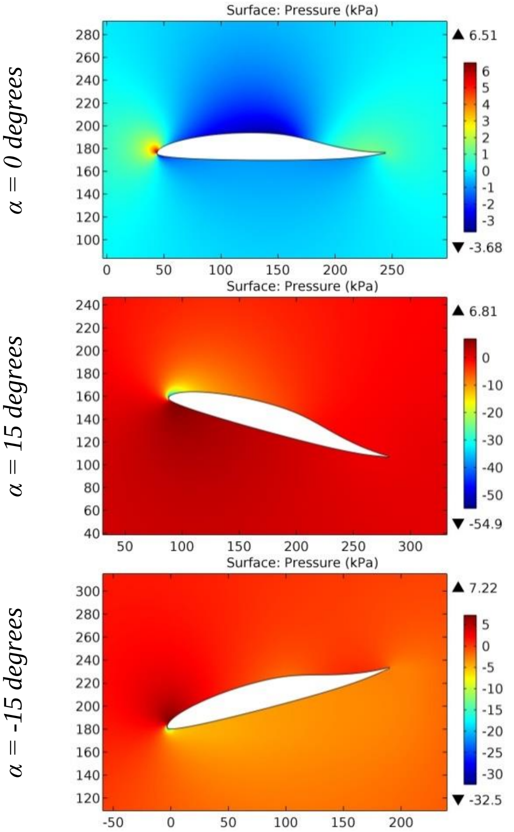

Figure 88. The pressure contours on the surfaces of the Roncz/Marske-7 airfoil.

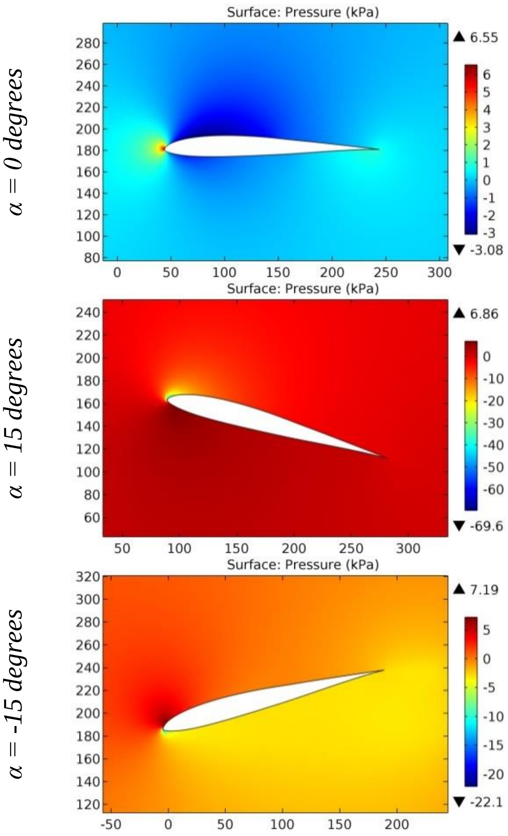

Figure 89. The pressure contours on the surfaces of the rs001 airfoil.

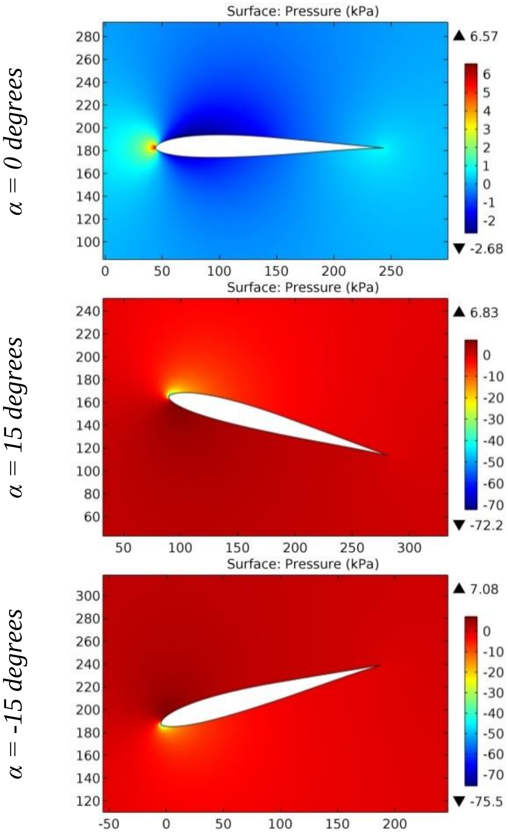

Figure 90. The pressure contours on the surfaces of the rs001m05 airfoil.

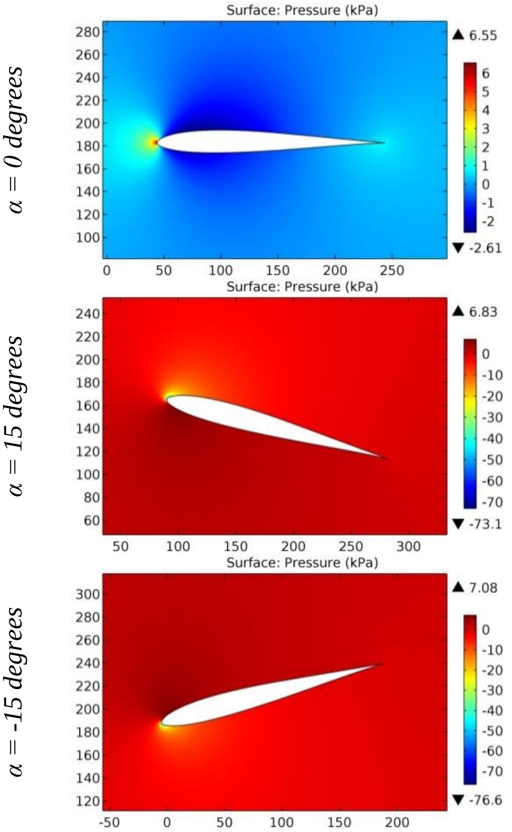

Figure 91. The pressure contours on the surfaces of the Rs001m60 airfoil.

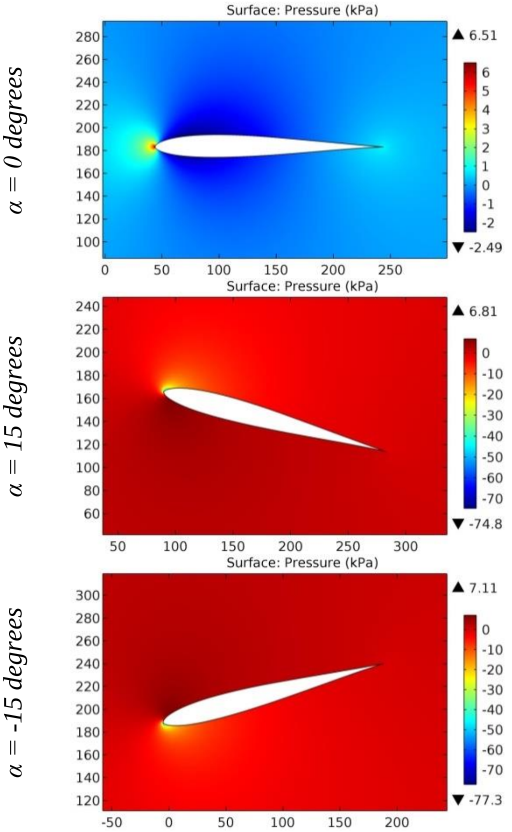

Figure 92. The pressure contours on the surfaces of the Rs001m75 airfoil.

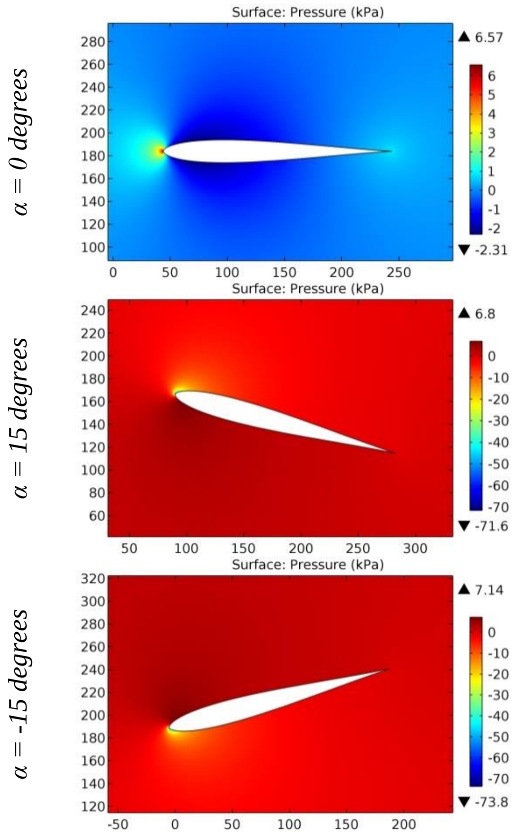

Figure 93. The pressure contours on the surfaces of the rs001t10 airfoil.

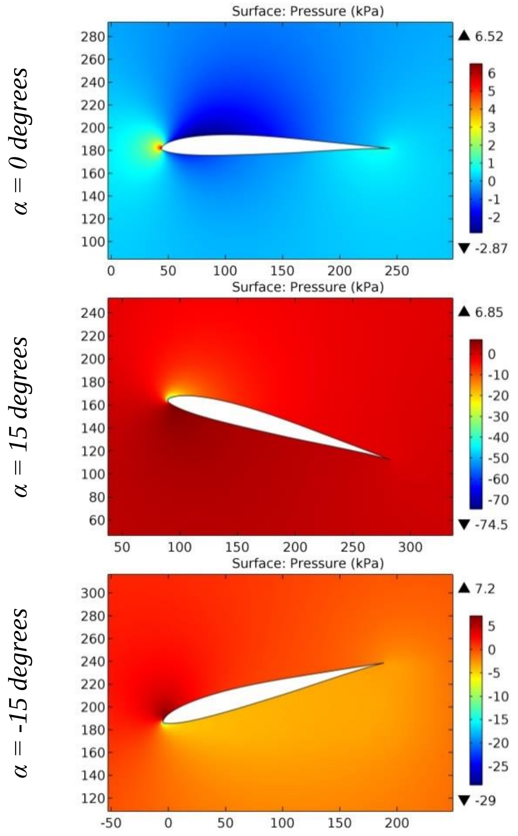

Figure 94. The pressure contours on the surfaces of the rs004a airfoil.

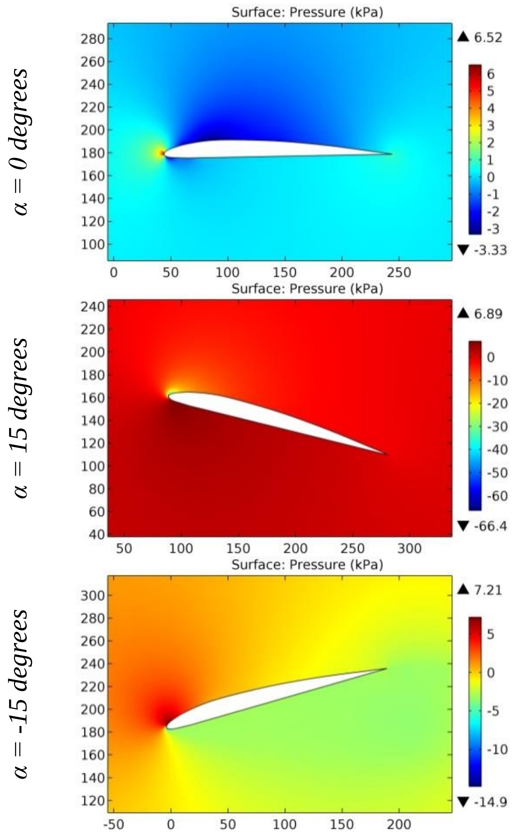

Figure 95. The pressure contours on the surfaces of the RSG-28 airfoil.

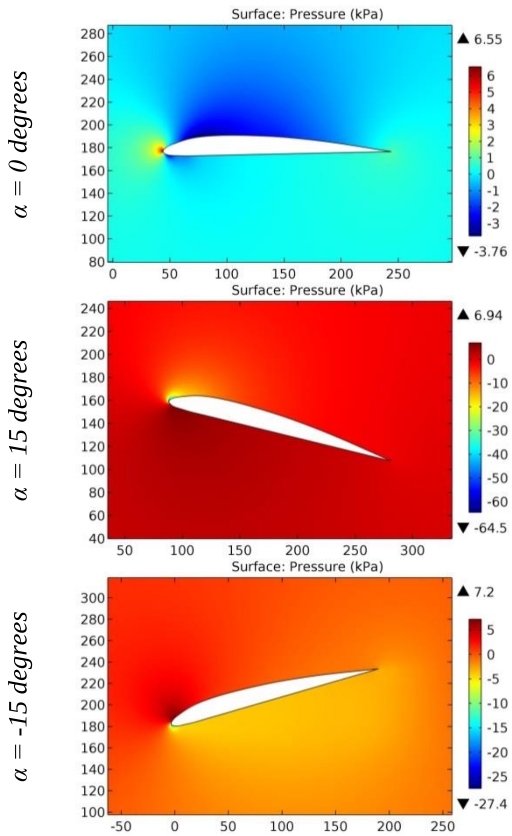

Figure 96. The pressure contours on the surfaces of the RSG-29 airfoil.

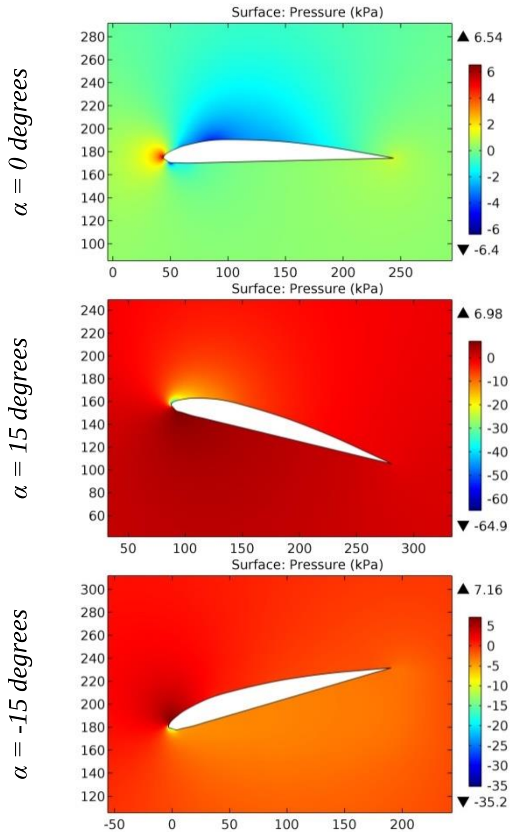

Figure 97. The pressure contours on the surfaces of the RSG-30 airfoil.

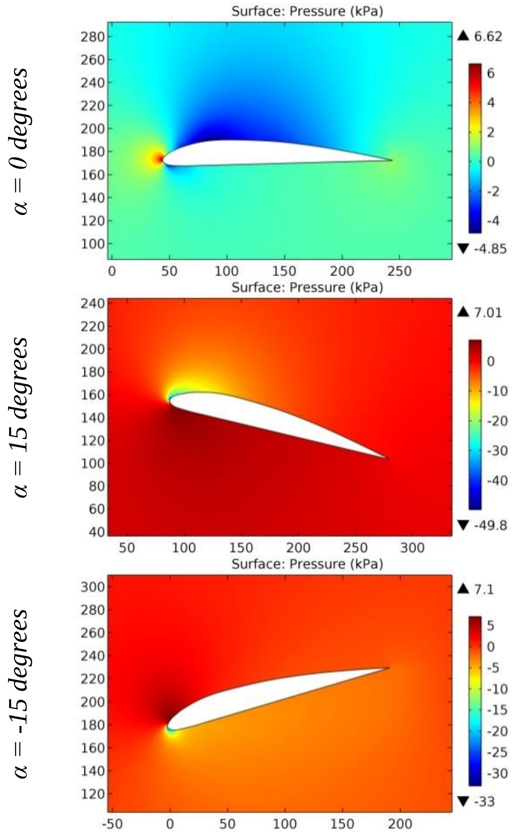

Figure 98. The pressure contours on the surfaces of the RSG-31 airfoil.

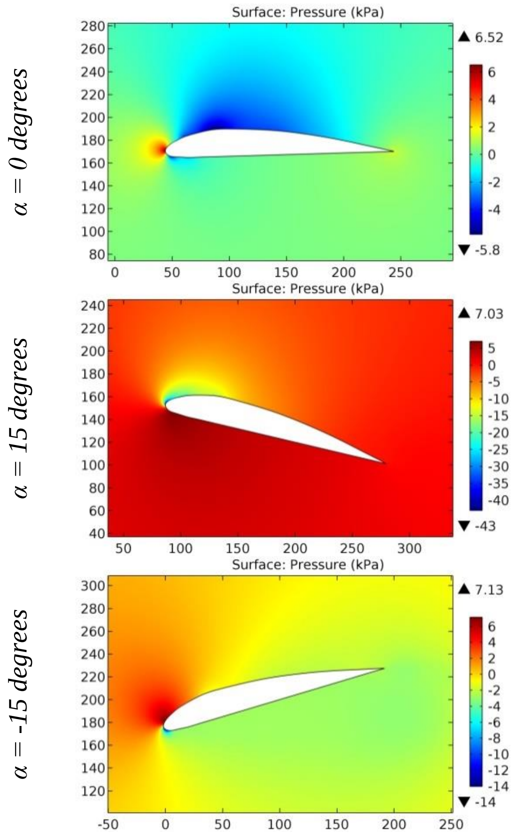

Figure 99. The pressure contours on the surfaces of the RSG-32 airfoil.

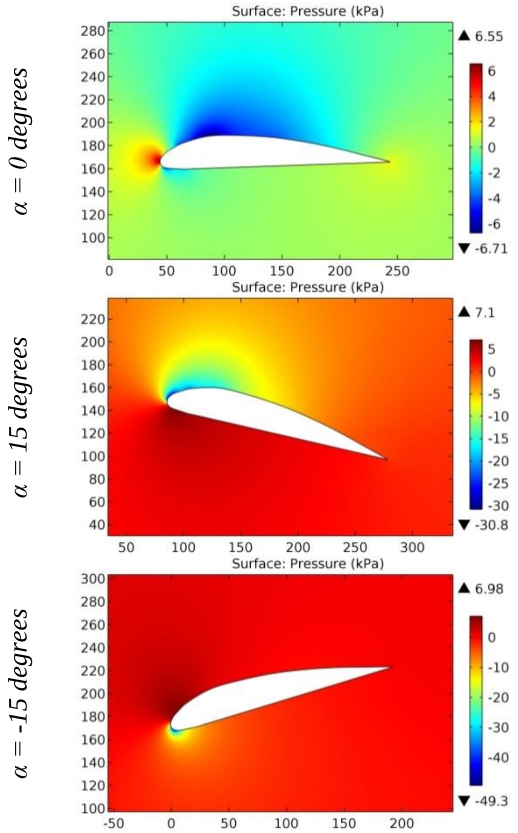

Figure 100. The pressure contours on the surfaces of the RSG-34 airfoil.

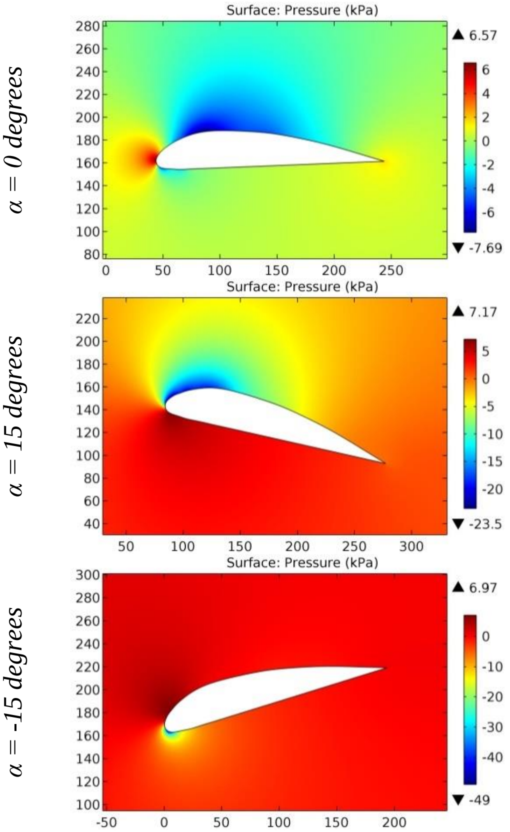

Figure 101. The pressure contours on the surfaces of the RSG-36 airfoil.

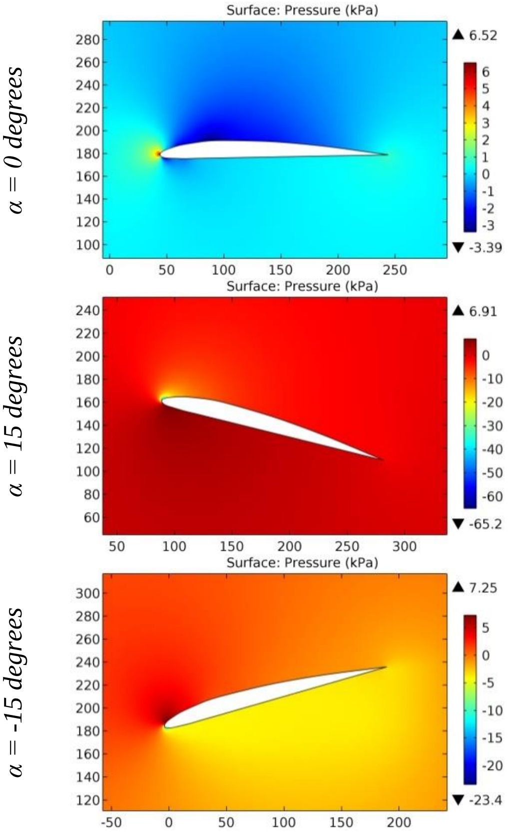

Figure 102. The pressure contours on the surfaces of the RSG-82 airfoil.

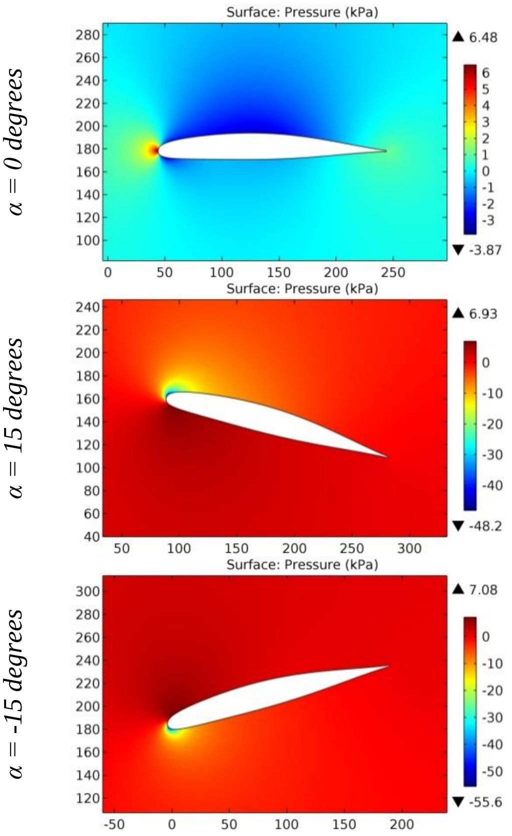

Figure 103. The pressure contours on the surfaces of the Rutan AMSOIL racer canard airfoil.

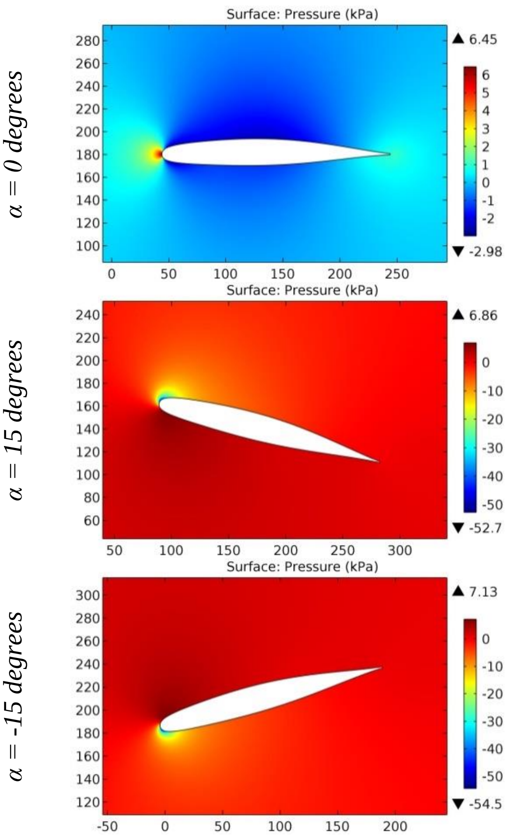

Figure 104. The pressure contours on the surfaces of the Rutan AMSOIL racer wing.

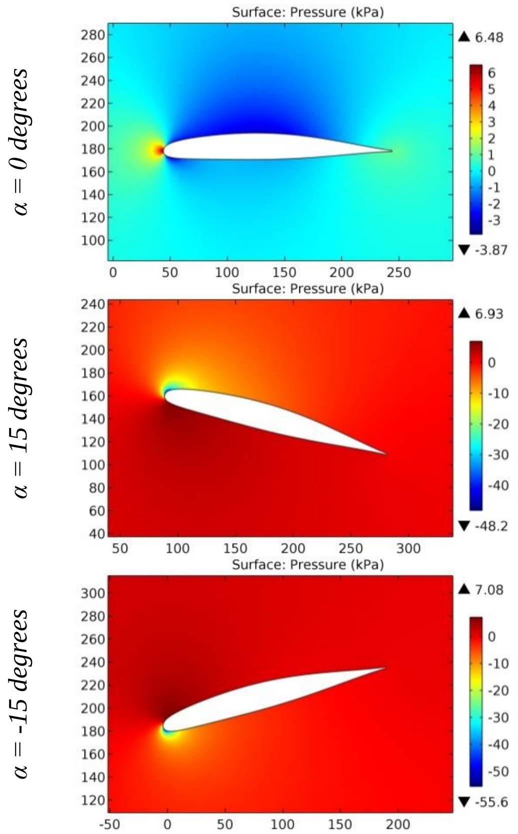

Figure 105. The pressure contours on the surfaces of the RUTAN CANARD airfoil.

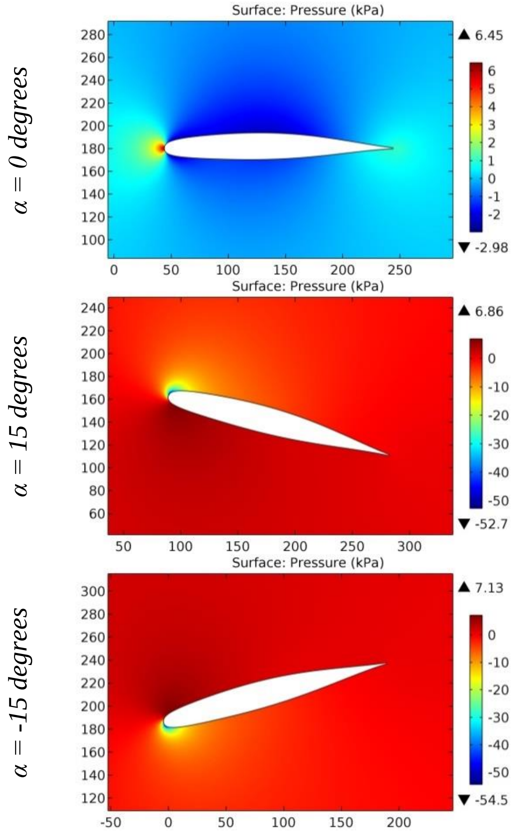

Figure 106. The pressure contours on the surfaces of the RUTAN WING.

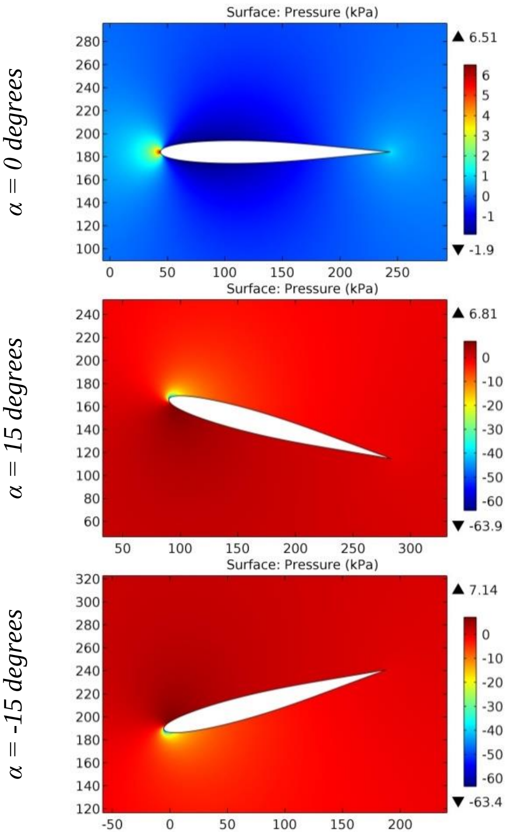

Figure 107. The pressure contours on the surfaces of the Ryan BQM-34 airfoil.

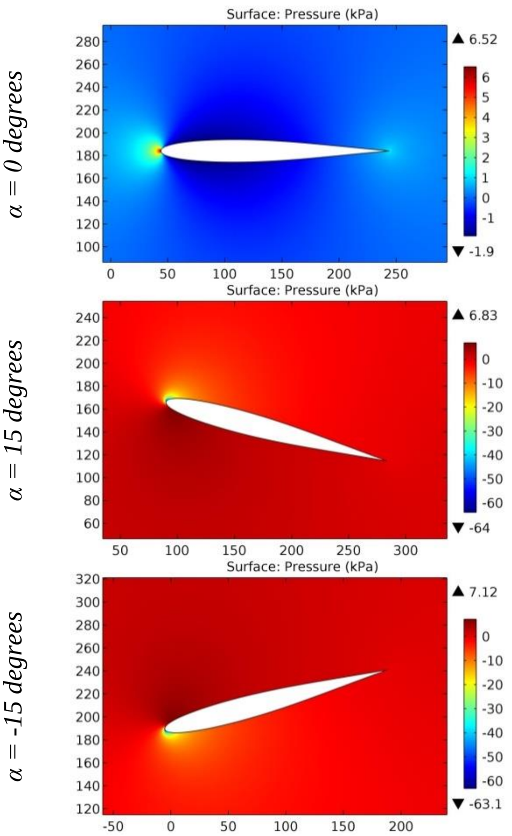

Figure 108. The pressure contours on the surfaces of the RYAN BQM-34 FIREBEE WING.

Pressures on the upper and lower surfaces of the airfoil during the airplane descent are almost the same in magnitude.

A similar pattern of pressure distribution on the upper and lower surfaces is observed at an angle of attack of -15 degrees of the Ritz 2-30-5 airfoil. The pressure difference is doubled during the airplane climb.

The greatest drag at an angle of attack of 15 degrees was determined for the Roncz/Marske-7 airfoil. Maximum pressure is formed on a small area of the leading edge of the airfoil.

The configuration of the RUTAN WING airfoil leads to the same magnitude of drag on the leading edge during the climb and descent of the airplane. Negative pressure acts on the upper and lower surfaces during the horizontal flight of the airplane.

Conclusion

Approximate values of the gradients of negative and positive pressures on the surfaces of the airfoils of the airplane wings were obtained on the basis of computer calculations. The analysis of the influence of the configuration of some airfoils on the magnitude of drag during the horizontal flight, climb and descent of the airplane within ±15 degrees was carried out. According to the presented largest and smallest values of pressures, it is possible to judge the lifting force of the airplane wing. The Rhode St Genese 26 and Ritz 2-30-5 airfoils are subjected to minimal stresses, which are affected by air flows at an angle of attack of -15 degrees.

References:

1. Anderson, J. D. (2010). *Fundamentals of Aerodynamics.* McGraw-Hill, Fifth edition.
2. Shevell, R. S. (1989). *Fundamentals of Flight.* Prentice Hall, Second edition.
3. Houghton, E. L., & Carpenter, P. W. (2003). *Aerodynamics for Engineering Students*. Fifth edition, Elsevier.
4. Lan, E. C. T., & Roskam, J. (2003). *Airplane Aerodynamics and Performance*. DAR Corp.
5. Sadraey, M. (2009). *Aircraft Performance Analysis.* VDM Verlag Dr. Müller.
6. Anderson, J. D. (1999). *Aircraft Performance and Design.* McGraw-Hill.
7. Roskam, J. (2007). *Airplane Flight Dynamics and Automatic Flight Control, Part I*. DAR Corp.
8. Etkin, B., & Reid, L. D. (1996). *Dynamics of Flight, Stability and Control.* Third Edition, Wiley.
9. Stevens, B. L., & Lewis, F. L. (2003). *Aircraft Control and Simulation.* Second Edition, Wiley.
10. Chemezov, D., et al. (2021). Pressure distribution on the surfaces of the NACA 0012 airfoil under conditions of changing the angle of attack. *ISJ Theoretical & Applied Science, 09 (101),* 601-606.
11. Chemezov, D., et al. (2021). Stressed state of surfaces of the NACA 0012 airfoil at high angles of attack. *ISJ Theoretical & Applied Science, 10 (102),* 601-604.
12. Chemezov, D., et al. (2021). Reference data of pressure distribution on the surfaces of airfoils having the names beginning with the letter A (the first part). *ISJ Theoretical & Applied Science, 10 (102),* 943-958.
13. Chemezov, D., et al. (2021). Reference data of pressure distribution on the surfaces of airfoils having the names beginning with the letter A (the second part). *ISJ Theoretical & Applied Science, 11 (103)*, 656-675.
14. Chemezov, D., et al. (2021). Reference data of pressure distribution on the surfaces of airfoils having the names beginning with the letter B. *ISJ Theoretical & Applied Science, 11 (103)*, 1001-1076.
15. Chemezov, D., et al. (2021). Reference data of pressure distribution on the surfaces of airfoils having the names beginning with the letter C. *ISJ Theoretical & Applied Science, 12 (104)*, 814-844.
16. Chemezov, D., et al. (2021). Reference data of pressure distribution on the surfaces of airfoils having the names beginning with the letter D. *ISJ Theoretical & Applied Science, 12 (104)*, 1244-1274.
17. Chemezov, D., et al. (2022). Reference data of pressure distribution on the surfaces of airfoils (hydrofoils) having the names beginning with the letter E (the first part). *ISJ Theoretical & Applied Science, 01 (105)*, 501-569.
18. Chemezov, D., et al. (2022). Reference data of pressure distribution on the surfaces of airfoils (hydrofoils) having the names beginning with the letter E (the second part). *ISJ Theoretical & Applied Science, 01 (105)*, 601-671.
19. Chemezov, D., et al. (2022). Reference data of pressure distribution on the surfaces of airfoils

having the names beginning with the letter F. *ISJ Theoretical & Applied Science, 02 (106)*, 101-135.

20. Chemezov, D., et al. (2022). Reference data of pressure distribution on the surfaces of airfoils having the names beginning with the letter G (the first part). *ISJ Theoretical & Applied Science, 03 (107)*, 701-784.
21. Chemezov, D., et al. (2022). Reference data of pressure distribution on the surfaces of airfoils having the names beginning with the letter G (the second part). *ISJ Theoretical & Applied Science, 03 (107)*, 901-984.
22. Chemezov, D., et al. (2022). Reference data of pressure distribution on the surfaces of airfoils having the names beginning with the letter G (the third part). *ISJ Theoretical & Applied Science, 04 (108)*, 401-484.
23. Chemezov, D., et al. (2022). Reference data of pressure distribution on the surfaces of airfoils having the names beginning with the letter H (the first part). *ISJ Theoretical & Applied Science, 05 (109)*, 201-258.
24. Chemezov, D., et al. (2022). Reference data of pressure distribution on the surfaces of airfoils having the names beginning with the letter H (the second part). *ISJ Theoretical & Applied Science, 05 (109)*, 529-586.
25. Chemezov, D., et al. (2022). Reference data of pressure distribution on the surfaces of airfoils having the names beginning with the letter I. *ISJ Theoretical & Applied Science, 06 (110)*, 1-7.
26. Chemezov, D., et al. (2022). Reference data of pressure distribution on the surfaces of airfoils having the names beginning with the letter J. *ISJ Theoretical & Applied Science, 06 (110)*, 18-25.
27. Chemezov, D., et al. (2022). Reference data of pressure distribution on the surfaces of airfoils having the names beginning with the letter K. *ISJ Theoretical & Applied Science, 07 (111)*, 1-10.
28. Chemezov, D., et al. (2022). Reference data of pressure distribution on the surfaces of airfoils having the names beginning with the letter L. *ISJ Theoretical & Applied Science, 07 (111)*, 101-118.
29. Chemezov, D., et al. (2022). Reference data of pressure distribution on the surfaces of airfoils having the names beginning with the letter M. *ISJ Theoretical & Applied Science, 10 (114)*, 307-392.
30. Chemezov, D., et al. (2022). Reference data of pressure distribution on the surfaces of airfoils having the names beginning with the letter N (the first part). *ISJ Theoretical & Applied Science, 12 (116)*, 801-892.
31. Chemezov, D., et al. (2022). Reference data of pressure distribution on the surfaces of airfoils having the names beginning with the letter N (the second part). *ISJ Theoretical & Applied Science, 12 (116)*, 901-990.
32. Chemezov, D., et al. (2023). Reference data of pressure distribution on the surfaces of airfoils having the names beginning with the letter O. *ISJ Theoretical & Applied Science, 01 (117)*, 624-635.
33. Chemezov, D., et al. (2023). Reference data of pressure distribution on the surfaces of airfoils having the names beginning with the letter P. *ISJ Theoretical & Applied Science, 02 (118)*, 48-61.